Cell Communication and Signaling

RESEARCH

Open Access

Herpes simplex virus-1 induces complement-mediated microglial phagocytosis of synapses in murine primary brain cultures and tissues

Mariya Timotey Miteva[1,2], Virginia Protto[3], Francesco Zanzi[1,2], Francesco Pastore[4,5], Chiara Simone[4,5], Cristian Ripoli[4,5], Maria Elena Marcocci[2], Roberto Piacentini[4,5], Claudio Grassi[4,5], Anna Teresa Palamara[2,3†] and Giovanna De Chiara[1*†]

Abstract

Background Numerous studies suggest that abnormal upregulation of the complement cascade, a key component of the innate immune system, is involved in the pathogenesis of Alzheimer's disease (AD), also contributing to synapse elimination in the brain. Several pieces of evidence suggest that recurrent herpes simplex virus-1 (HSV-1) infection reaching the brain is one of the AD risk factors, including those reporting synaptic loss and consequent cognitive deficit following multiple virus replication in the brain. However, the role of complement cascade activation in such events remains unexplored.

Methods Murine primary neurons co-cultured or not with microglial BV2 cells and organotypic hippocampal brain slices were used as experimental models of HSV-1 infection. Virus effects on complement cascade activation and synaptic loss were assessed by evaluation of protein and mRNA levels of specific complement components and synaptic markers. Confocal immunofluorescence microscopy was used to analyze microglial phagocytosis of synapses. To evaluate the role of complement cascade activation in such event, experimental models were treated with a neutralizing anti-C3 antibody within the infection. Two-photon imaging and patch-clamp recordings of organotypic hippocampal slices were used to quantify dendritic spine density on secondary apical dendrites of CA1 pyramidal neurons and synaptic transmission.

Results We first found that HSV-1 infection significantly upregulates the expression of components of the classical complement cascade at both mRNA and protein levels, and promotes their localization at synapses. Then, we provide evidence that HSV-1 infection causes increased microglial phagocytosis of synapses, which is partially prevented when the complement cascade is inhibited. Furthermore, by exploiting murine organotypic hippocampal slices, we confirmed that the virus triggers synaptic damage through microglial pruning of synapses via a complement-dependent mechanism. Importantly, in infected CA1 neurons, we detected a significant decrease in spine density,

†Anna Teresa Palamara and Giovanna De Chiara contributed equally to this work.

*Correspondence:
Giovanna De Chiara
giovanna.dechiara@ift.cnr.it

Full list of author information is available at the end of the article

which was paralleled by functional alterations in synaptic transmission. Both events were rescued when infection is performed in the presence of an antibody neutralizing the complement C3 protein.

Conclusion Our data indicate that HSV-1 infection triggers aberrant complement activation and complement-mediated microglial engulfment of damaged synapses, further supporting the role of HSV-1 in neurodegeneration.

Plain English summary

Herpes simplex virus type 1 (HSV-1), a neurotropic and widespread pathogen, has been suggested as a potential risk factor for Alzheimer's disease (AD), the most common form of dementia in elderly people. However, the molecular mechanisms triggered by the virus remain to be fully elucidated. Increasing evidence suggests that the innate immune system, particularly the complement cascade, plays a key role in early synapse loss, a hallmark of AD progression. Here, we demonstrate that HSV-1 infection of brain cells induces upregulation of complement components, promoting complement-dependent microglia engulfment, thus contributing to synaptic loss. Our results support a causative role of complement in HSV-1-induced synaptic pruning thus providing a novel understanding of how HSV-1 infection contributes to synaptic loss in AD.

Keywords HSV-1, HHV-1, Herpes simplex virus, Complement proteins, Microglial synaptic pruning, Alzheimer's disease, Neurodegeneration

Background

The complement system is an important player in the innate immune response, especially for the protection against pathogen invasion and the clearance of damaged cells [1, 2]. It also plays a key role in the synaptic pruning occurring during physiological brain development [3, 4], when the excess of synapses and the resulting extra connections must be removed to form a mature brain with a well-functioning neuronal network. Specifically, in the developing central nervous system (CNS), the complement components C1q, C3, and C4 localize at synapses, tagging them for potential microglia phagocytosis [5, 6]. Microglia cells are indeed the effectors of this process since, by expressing the complement receptor 3 (CR3), they can interact with C3 at the synapses to initiate their engulfment [7]. Interestingly, this process also occurs in the adult brain, where its hyperactivation may lead to severe neurological disorders. Increased expression of C4 has been associated with a greater risk for schizophrenia [5], whereas classical complement pathway activation and altered phagocytosis were found in human brain samples of epileptic patients [8]. Detrimental complement-dependent synaptic elimination has been described in an in vivo mouse model after acute brain infection of neuroinvasive viruses such as Zika virus and West Nile virus [9–11], whose damaging effects in the CNS are well-known. Along this line, recent studies have also shown that some respiratory viruses, including severe acute respiratory syndrome coronavirus 2 (SARS-CoV-2) and influenza A virus, may trigger complement-dependent synaptic elimination following acute infection [12, 13], suggesting this as a possible mechanism underlying their neurovirulence.

Notably, aberrant complement cascade activation has been more recently associated with the progression and pathogenesis of Alzheimer's disease (AD) [14], the most common form of dementia in elderly people [15], that is strongly characterized by brain accumulation of misfolded proteins such as amyloid-β (Aβ) and hyperphosphorylated tau, synaptic loss and consequent cognitive deficit [15, 16]. Different studies have highlighted increased levels of complement proteins in the cerebrospinal fluid (CSF) of AD patients, confirming that aberrant activation of the complement cascade occurs in the AD brain [17, 18]. Furthermore, in AD mouse models, complement and microglia have been shown to mediate synaptic loss, thus contributing to neurodegeneration. In particular, in the J20 mouse model, characterized by Aβ hyperproduction and plaque deposition, increased levels of C1q were found at synapses in an early phase of the disease (i.e., before plaque formation), and inhibition of C1q, C3 or microglial receptor CR3 resulted in the reduction of microglial-mediated synapse phagocytosis [14, 19].

A growing body of evidence supports a possible role of herpes simplex virus-type 1 (HSV-1) in AD pathogenesis, especially those shedding light on the molecular mechanisms underlying the harmful effects of repeated mild infections in the brain (reviewed in [20]). HSV-1 is indeed a neurotropic virus that usually establishes a life-long latent infection in humans with periodic reactivations that may occasionally spread to the CNS. Herein, the virus induces a strong inflammatory response resulting in either severe herpetic encephalitis (HSE) or asymptomatic mild infections producing small damage that may eventually lead to long-term neurodegeneration. We previously reported that HSV-1 induces: (i) the amyloidogenic processing of amyloid precursor protein (APP) triggering Aβ production and accumulation; (ii) activation of kinase pathways involved in tau protein hyperphosphorylation; (iii) neuroinflammation; (iv) impaired neurogenesis; (v) epigenetic alterations; (vi) synaptic and memory deficits [21–25]. More recently, we

evidenced that the virus exploits extracellular vesicles (EV) to spread neurotoxic proteins among brain cells [26] and highlighted the role of interleukin 1β (IL-1β), a key mediator in the immune response, in the synaptic deficits induced by recurrent HSV-1 brain infection in mice [27].

In the present study, we further investigated the molecular mechanism underlying HSV-1-induced synaptic dysfunction, focusing on the potential role of complement proteins. In primary cultures of murine brain cells, we first found that the virus strongly upregulates the expression levels of the components of the classical complement cascade, promoting their localization at synapses. Our results from engulfment assay and confocal immunofluorescence analyses (IF) also indicated that HSV-1 infection triggers increased microglial phagocytosis of synaptic materials, which is partially prevented when the complement cascade is inhibited. Finally, by exploiting organotypic hippocampal slices as an ex vivo model of HSV-1 brain infection, we confirmed that the virus triggers microglial pruning of synapses by activating the C3-dependent pathway, which results in excitatory synaptic signalling alteration. Our data provide novel evidence that HSV-1 contribution to neurodegeneration includes microglial-mediated synaptic damage via a complement-dependent mechanism.

Methods

Ethics statement

Animals were purchased from Charles River Laboratories. All the experimental protocols used in the present study complied with the European Guide for the Care and Use of Laboratory Animals and institutional guidelines and with the Italian legislation on animal experimentation (Decreto legislativo n. 26/2014, Direttiva UE 63/2010). Experimental protocols were reviewed by the Animal Welfare Body (Istituto Superiore Sanità and Università Cattolica) and authorized by the Italian Ministry of Health (code numbers D9997.N.GRQ, D9997.N.J9T, and 934/2021-PR).

Cell lines

Human SH-SY5Y neuroblastoma (ATCC CRL-2266) was grown in Dulbecco's modified Eagle's medium (DMEM, Euroclone) containing 10% heat-inactivated fetal bovine serum (FBS, Good, Bio-Cell), glutamine (2 mM), penicillin (100 units/ml), and streptomycin (100 µg/ml). African green monkey kidney VERO cells (ATCC CCL-81) were maintained in RPMI 1640 medium (Gibco) supplemented with 10% FBS, antibiotics, and glutamine (2 mM). The BV2 murine microglial cell line (ICLC ATL03001) was obtained from the Interlab Cell Line Collection (ICLC), Cell Bank of Genoa, Italy, and kindly provided by Prof. Maria D'Erme, Sapienza University of Rome. Cells were cultured in DMEM, supplemented with 10% FBS, 1% penicillin-streptomycin, and glutamine (2 mM). All cells were cultured at 37 °C in a humidified incubator under 5% CO_2.

Primary neuronal cultures and their co-cultures with microglia

Primary cultures of cortical neurons were prepared from WISTAR E17 rat embryos, or C57BL/6 E17 mouse embryos (Charles River Laboratories) as previously described [23]. Briefly, the embryos were decapitated to separate the head from the rest of the body, then the brains were dissected to isolate the cortices, including the hippocampus regions. After removing the meninges, the cortices were collected in cold PBS and then incubated for 15 minutes (min) at 37 °C in trypsin-EDTA (0.025%/0.01%; 500 µl/brain, Gibco). After blocking trypsin with FBS, the tissues were mechanically dissociated at room temperature (RT) with a sterilized Pasteur pipette, and the cell suspension was centrifuged at 1200 rpm for 3 min. The pellet was suspended in Minimum Essential Medium (MEM; Sigma-Aldrich) containing 5% FBS, 5% horse serum, 1% glutamine (2 mM), 1% penicillin-streptomycin-neomycin antibiotic cocktail (PSN, Sigma-Aldrich) and glucose (25 mM). Cells were plated at a density of 8×10^5 cells/well in 2 ml of the above indicated medium on 6-well plates or at 0.4×10^5 cell/well in 1 ml of medium on 24-well plates (for immunofluorescence analyses), or at 2.5×10^4 cells/well in 0.1 ml medium on 96 well-plates (for cell viability assay), all pre-coated with poly-L-lysine (0.1 mg/ml; Sigma-Aldrich), and maintained in a humidified incubator at 37 °C, 5% CO_2. Four to six hours (h) later, the culture medium was replaced with Neurobasal medium (Gibco) containing 2% B-27 (Invitrogen), 2 mM glutamine, and 1% PSN. Four days after plating, the medium was replaced with Neurobasal medium devoid of glutamine and supplemented with 2% B-27 and 1% PSN. Neurons were cultured for 12–13 days, changing half of the medium every 48 h and then HSV-1 or mock-infected at Days in vitro (DIV) 13. For co-culture experiments, microglial BV2 cells were added to mouse primary neuronal cultures at DIV 12 in a 5:1 ratio (neurons:microglia). After 24 h (DIV 13), co-cultures underwent HSV-1 or mock infection as described below.

Organotypic hippocampal slice cultures

Hippocampal organotypic slice (350 µm) cultures were prepared from postnatal day 2–8 mice through a McIlwain tissue chopper and placed on semi-porous membranes (Millipore) as previously described [28]. One day after the slices preparation, the EGFP plasmid was biolistically transfected by using the Gene-Gun system (Bio-Rad Laboratories) [29]. After 48 h of transfection, the slices were treated for 4 h prior to HSV-1 or mock infection with anti-C3 antibody (C3 Ab) (sc-28294, mouse

IgG1 isotype, Santa Cruz) or vehicle, then two-photon live imaging experiments were carried out after 48 h of infection. For electrophysiological studies, 3 days after preparation, slices were treated for 4 h prior to HSV-1 or mock infection with C3 Ab, or control IgG (sc-3877, mouse IgG1 isotype, Santa Cruz) or vehicle, then whole-cell patch-clamp recordings were performed 48 h post infection (p.i.).

Virus production and titration, and infection

HSV-1 (strain F, wild-type, a kind gift from Prof. Manservigi, Ferrara University, Italy) production was performed by infecting at 0.01 multiplicity of infection (MOI) VERO cells cultured in 75-cm^2 tissue culture flasks. After 48 h at 37 °C and 5% CO2, the HSV-1-infected cells underwent 3 freeze/thaw cycles, and cell debris were removed by low-speed centrifugation. The virus-containing supernatant was collected and titered by Standard Plaque Assay (SPA [30]), as plaque-forming units (PFU) per ml (PFU/ml). Briefly, serial viral or infected-supernatant dilutions were incubated for 1 h with confluent VERO cell monolayers in 24-well plates. Supernatants were discarded and the VEROs were subjected to a washing step in Dulbecco's Phosphate Buffered Saline (PBS, without calcium chloride and magnesium chloride, Sigma-Aldrich). Then, PBS was replaced with RPMI medium supplemented with 2% FBS and 2% carboxymethylcellulose (CMC, Sigma-Aldrich) to contain the viral infection. After 48 h, the VERO cells were fixed in absolute methanol and stained with 0.5% crystal violet solution (Sigma-Aldrich) for 15 min and then extensively washed to evaluate plaque formation. In this study, the virus had a 1.7×10^8 PFU/ml titer. Similarly, a mock solution (mock or ctr within the text) was prepared from uninfected VERO cells.

HSV-1 infection of SH-SY5Y cells

Twenty-four h after SH-SY5Y plating, cells were challenged with HSV-1 (3 MOI) for 1 h at 37 °C, washed with PBS, and then incubated with medium supplemented with 2% FBS. Analyses were performed 24 h p.i. Supernatants of each infection were titered by SPA.

HSV-1 infection of primary cultures and their co-cultures with BV2

For primary cultures, after 13 days from plating (DIV13), the conditioned medium (CM) was removed and cells were inoculated with 1 or 3 MOI of HSV-1 in Neurobasal medium for 1.5 h at 37 °C. The medium was then removed and after washing with PBS, the cells were returned to their original CM. After 24 h, the supernatant was harvested for titration by SPA. For co-cultures experiments, HSV-1 or mock infection were performed at DIV 13, one day after BV2 addition. For complement inhibition experiments, co-cultures were treated with 1 µg/ml C3 Ab or 1 µg/ml control IgG isotype (IgG) within 24 h after virus or mock inoculation. Supernatants of each infection were titered by SPA.

HSV-1 infection of organotypic hippocampal brain slices

Three days post-transfection or 3 days after preparation, the organotypic brain slice cultures were infected with HSV-1 (1×10^5 PFU/brain slice). Forty-eight h p.i., brain slices analyzed for spine density or electrophysiological studies (see below), or collected and stored at – 80 °C for western blot analyses (WB, see below) or fixed with 4% paraformaldehyde in PBS for confocal immunofluorescence analyses (IF, see below). For inhibiting complement activation, organotypic slices were treated with C3 Ab, control IgG or vehicle 4 h before HSV-1- or mock- infection and within the 48 h of infection.

Synaptosome isolation and phagocytosis assay

Isolation of synaptosomes was performed as previously described [31] with minor modifications. Briefly, neuronal cultures were homogenized in cold Buffer A (5 mM Hepes, 5 mM EGTA, 0.32 M sucrose) containing 1mM Na_3VO_4, 0.1mM PMSF and 0.1x Complete Protease Inhibitor Cocktail and Phosphatase Inhibitor Cocktail 1 and 2 (Sigma-Aldrich) and centrifuged at 2000 rpm to remove nuclei and large debris (P1). The supernatant (S1) was centrifuged at 11000×g to obtain crude synaptosomal fraction (P2), which was washed with TBS and lysed in RIPA buffer (40 mM Tris, 300 mM NaCl, 2% Triton X-100, 2% sodium deoxycholate, 0.2% SDS) containing protease and phosphatase inhibitor cocktail (Sigma-Aldrich) for WB analyses or and subsequently resuspended in DMEM for the engulfment assay with BV2 microglial cells or characterized with synaptophysin or PSD-95 content by confocal immunofluorescence (IF), see below.

For phagocytosis assay, synaptosomes isolated from mock or HSV-1 infected primary cultures were added to BV2 cells (60000/well) in poly-L-lysine-coated 24-well plates containing coverslips for IF. Two h after the addition of synaptosomes cells were fixed with ice-cold methanol and stained for PSD-95 for IF analyses (see below).

Western blotting

Cells, synaptosomes and organotypic brain cultures were lysed in RIPA buffer (20 mM Tris, 150 mM NaCl, pH 7.4, 1% Triton X-100, 1% sodium deoxycholate, 0.1% SDS) containing 5 µM sodium butyrate and protease and phosphatase inhibitors cocktails (Sigma-Aldrich). After 30 min incubation on ice, cell debris were eliminated by centrifugation at 14000 rpm at 4˚C for 20 min. Total protein concentrations were measured with Micro BCA method (Thermo Fisher Scientific). Equal amount of protein samples (35 µg) was separated by 7.6–15%

SDS-PAGE and blotted onto 0.22/0.45 μm nitrocellulose membrane (Bio-Rad; GE Healthcare). Membranes were coloured with Ponceau Red (Sigma-Aldrich) and, after washing with TBS (Tris buffered saline), blocked in 10% non-fat milk (1–2 h), in 0.1% Tween-20 TBS (T-TBS). Only for C3 protein detection, membranes were blocked in 5% BSA in T-TBS. Then, the filters were incubated overnight at 4˚C with the primary antibody (Ab) diluted in 5% non-fat milk in T-TBS. C3 Ab was diluted in 2.5% BSA in T-TBS. We used the following dilution for primary Abs: anti-C1q Ab 1:1000 (ab189922, Abcam); anti-C3 Ab 1:400 (sc-28294, Santa Cruz); anti-PSD-95 Ab 1:1000 (MA1-045, Thermo Fisher Scientific); anti-Synaptophysin Ab 1:1000 (A6344, Abclonal); anti-SMC3 Ab 1:3000 (A19591, Abclonal); anti-β-actin Ab 1:5000 (A2228, Sigma-Aldrich). After 3 × 10 min washes with T-TBS, the membranes were incubated for 1 h with secondary Ab (horseradish peroxidase-conjugated antibodies, Jackson Immuno Research Laboratories), followed by 3 × 10 min washes in T-TBS. The chemiluminescence reaction was obtained using Clarity or Clarity Max Western ECL Substrate (Bio-Rad) and detected by Chemidoc Imaging System (Bio-Rad Laboratories). Densitometric analysis was performed using ImageJ Software. The integrated density, corrected for non-specific background, was normalized to equal loading of the housekeeping protein β-actin. Full Uncropped Gel and Blot images_S1 Data shows the whole uncropped images of original WB from which figures have been derived.

Confocal immunofluorescence microscopy

Rat primary cultures and co-cultures of mouse primary neurons and BV2 cells

Primary cultures and co-cultures of brain cells, were processed for confocal immunofluorescence microscopy according to a standard protocol [21]. Briefly, cells were fixed with 4% paraformaldehyde (Sigma-Aldrich) in PBS for 10 min at RT rinsed twice in PBS, and permeabilized by 10 min incubation with 0.1% Triton X-100 in PBS. For PSD-95 immunostaining, cells were fixed in ice-cold methanol for 10–20 min at 4˚C. Cells were then blocked for 60 min in 0.1% horse serum (16050130, Gibco), 0.1% tween (Tween 20, 1706531-Bio- Rad Laboratories) in PBS and incubated overnight at 4 °C with different pairs of the following Abs: anti-C1q Ab 1:1000 (ab189922, Abcam); anti-C3 antibody 1:1000 (sc-28294, Santa Cruz); anti-NeuN Ab 1:300 (MAB377, Millipore, Sigma-Aldrich); anti-PSD-95 Ab 1:400 (51-6900, Thermo Fisher Scientific); anti-CD68 Ab 1:500 (clone FA-11, Bio-Rad Laboratories). The following day, cells were washed twice in PBS and then incubated for 90 min at room temperature with a mixture of the following secondary Abs: donkey anti-rabbit Alexa Fluor 488 (1:800; Invitrogen/Thermo Fisher Scientific), donkey anti-mouse Alexa 546 (1:800, Invitrogen/Thermo Fisher Scientific), Cy3 donkey anti-rat 1:200 (712-165-150, Jackson ImmunoResearch) Abs. Nuclei were then counterstained for 10 min with DAPI (1 μg/ml) and the cells were coverslipped with Fluoromount-G (004958-02, Invitrogen/Thermo Fisher Scientific). Images were acquired at 20x or 40x/63x magnification with oil-immersion objectives of a confocal laser scanning system (Leica SP5 and Leica Stellaris), under a sequential mode to avoid a crosstalk between channels. Quantification of immunofluorescence total signals was carried out using the ImageJ software (NIH) by drawing regions of interest (ROIs) and quantifying the mean fluorescence intensity in the ROIs of the selected channel. $CD68^+$ cells were manually counted. Quantification of immunofluorescence for colocalization measurements was carried out using ImageJ software, masking both red and green channels (CD68 and PSD95) with a fixed threshold and quantifying the area where both signals co-occurred in every images.

Synaptosomes and engulfment assay

For synaptosome characterization, P2 fractions isolated from mouse primary neuronal cultures were plated onto poly-L-lysine–coated glass coverslips (0.1 mg/ml) and allowed to adhere for 2 h. Samples were then fixed with ice-cold methanol for PSD-95 immunostaining or with 4% paraformaldehyde for synaptophysin immunostaining, followed by permeabilization and immunofluorescence staining performed as described above, using anti-PSD-95 or anti-synaptophysin antibodies (1:500; A6344, Abclonal). For engulfment assay, BV2 supplemented with isolated synaptosome, as described above, were fixed in ice-cold methanol for 10–15 min at 4˚C. Cells were then blocked for 60 min in 0.1% horse serum, 0.1% tween in PBS and incubated at 4 °C in the same buffer overnight at 4 °C with anti-PSD-95 1:500 (51-6900, Invitrogen/Thermo Fisher Scientific); anti-CD68 Ab 1:500 (clone FA-11, Bio-Rad Laboratories). The following day, cells were washed twice in PBS and then incubated for 90 min at RT with a mixture of the following secondary antibodies: donkey anti-rabbit Alexa Fluor 488 (1:800; Invitrogen), Cy3 donkey anti-rat 1:100 (712-165-150, Jackson ImmunoResearch) Abs. Nuclei were then counterstained for 10 min with DAPI 1 μg/ml and the cells were coverslipped with Fluoromount-G (004958-02, Invitrogen/Thermo Fisher Scientific). Images were acquired with a confocal laser scanning system (Leica Stellaris).

Organotypic hippocampal slice cultures

Forty-eight h p.i., organotypic slices were fixed overnight at 4 °C with 4% paraformaldehyde in PBS. The following day, slices were incubated with a blocking buffer containing 3% horse serum and 2% Triton-X 100 in PBS for 2 h at RT. Then, slices were treated with one of the following

Abs diluted in PBS containing 1% horse serum, and 0.5% Triton-X 100: anti-CD68 1:200 (clone FA-11, Bio-Rad Laboratories) and anti-total HSV-1 Abs 1:300 (Bio-Rad Laboratories) for 48 h at 4 °C. Then, after 4 washes with PBS (10 min each), slices were incubated with secondary Abs such as, donkey anti-goat Alexa 647 (1:500, Invitrogen/Thermo Fischer Scientific) and Cy3 donkey anti-rat 1:100 (712-165-150, Jackson ImmunoResearch) Abs for 2 h at RT and nuclei were counterstained with DAPI (5 µg/ml). Finally, slices were coverslip with ProLong Glass Antifade Mountant (P36980, Invitrogen/Thermo Fisher Scientific). Images were acquired again with confocal laser scanning system (Leica SP5 and Leica Stellaris). For total organotypic slices, images were acquired at 20x under navigator merging function. For colocalization measurements, Z-stacks of 5 images acquired every 0.5 µm were acquired with 63x objective. Quantification of immunofluorescence was carried out using the ImageJ software by masking both red and green channels (CD68 and EGFP fluorescence) and quantifying the area where both signals co-occurred in every image of the acquired Z-stack. Data of single images were then pooled together thus obtaining the final data for each Z-stack. For figure production, Z-stacks of 20 images spanning every 0.25 µm were acquired.

Cell viability assay

Cell viability was assessed using the MTT assay. Primary neuronal cultures supplemented with microglia were seeded in multiwell plates and maintained at 37 °C in a humidified 5% CO_2 atmosphere. Twenty-four h later, cells were treated with 1 µg/ml C3 Ab or 1 µg/ml IgG or vehicle for 24 h. Then, MTT reagent (Sigma-Aldrich, M-5655) was added to the cultures at a final concentration of 0.5 mg/mL and incubated for 4 h to allow the formation of formazan crystals. The medium was then carefully removed, and formazan was solubilized by addition of DMSO. After incubation at 37 °C, absorbance was measured at 570 nm using a microplate reader. For assessment of cell viability following HSV-1 infection, the same procedure was performed following 24 h of 3 MOI HSV-1 or mock solution inoculation. Cell viability was expressed as a percentage relative to untreated or mock controls.

RT-PCR analyses

Nucleic acids were extracted from mouse brains using a one-step method (Total RNA Purification Plus Kit, 48400, Norgen Biotek Corp) according to the manufacturer's protocols, and their concentrations were assessed spectrophotometrically. Total RNA was reverse transcribed in cDNA using SensiFAST cDNA synthesis kit (BIO 65053, Meridian Bioscience) according to the manufacturer's recommendations. RT-PCR was then performed with the iTaq™ Universal SYBR® Green Supermix (1725121 Bio-Rad Laboratories) on a iQ5 Real-Time PCR Detection system (Bio-Rad Laboratories) or StepOnePlus Applied Biosystems™ Real-Time PCR Systems to amplify C1q, C3, PSD-95,IL-1β, interleukin-6 (IL-6), inducible nitric oxide synthase (iNOS), interleukin-10 (IL-10), Arginase 1 (Arg1), CD206, Glyceraldehyde-3-phosphate dehydrogenase (GAPDH) and β-actin. The PCR reaction (95 °C for 5 min, followed by 35 cycles of 95 °C for 15 seconds (s), 57 °C/60°C for 30 s was performed with the following primers (at 300 nM): A) C1q forward: CGACTATGCCC AAAACACCT; C1q reverse: GGAAAAGCAGAAAGCC AGTG [32]. B) C3 forward: ACC TTA CCT CGG CAA GTT TCT; C3 reverse: TTG TAG AGC TGC TGG TCA GG [33]. C) PSD-95 forward: ACAACCAAGAAATACC GCTACCA; PSD-95 reverse: CCCCTCTGTTCCATTCA CCTG [34]. D) IL-1β forward: CAAGCTTCCTTGTGC AAGTGTC; IL-1β reverse: TTCATCTTTTGGGGTCC GTCA. E) IL-6 forward: CCACTTCACAAGTCGGAGG CTTA; IL-6 reverse: GCAAGTGCATCATCGTTGTTC ATAC [35]. F) iNOS forward: CCCTTCAATGGTTGGT ACATGG; iNOS reverse ACATTGATCTCCGTGACAG CC [36]. G) IL-10 forward: GCTCTTACTGACTGGCA TGAG; IL-10 reverse: CGCAGCTCTAGGAGCATGTG [36]. H) Arg1 forward: CTC CAA GCC AAA GTC CTT AGAG; Arg1 reverse: GGA GCT GTC ATT AGG GACA TCA [36]. I) CD206 forward: ATC CAC TCT ATC CAC CTT CA, CD206 reverse: TGC TTG TTC ATA TCT GTC TTCA [37]. J) GAPDH forward: AACCTGCCAAG TATGATG, GAPDH reverse: GGAGTTGCTGTTGAAG TC [38]. K) Actin forward: AGG CAT CCT CAC CCT GAA GTA, Actin reverse: CAC ACG CAG CTC ATT GTA GA-3 [39].

Duplicates were run for each sample. Cycle threshold (Ct) values achieved were normalized to the endogenous control actin or GAPDH, and the $2^{-\Delta\Delta Ct}$ method [40] was used for the comparative analyses. Results were reported as mean ± SEM and calculated as fold-change of gene expression vs. controls.

ELISA

For quantification of a possible C3 release after infection, supernatants from HSV-1-infected (at 3 MOI) rat primary cultures were harvested 24 h p.i., centrifuged at 1200 rpm for 30 min at 4 °C to eliminate cell debris, and then analyzed by ELISA Assay (ab157731- Abcam) according to manufacturer's instructions.

Two-photon laser-scanning imaging for dendritic spine counting

Transfected organotypic hippocampal slice cultures were transferred to a recording chamber and immersed in artificial cerebrospinal fluid (ACSF) containing (in mM): 119 NaCl, 2.5 KCl, 4 $CaCl_2$, 4 $MgCl_2$, 1 NaH_2PO_4,

26 $NaHCO_3$, 11 D-glucose, gassed with 95% O_2/5% CO_2. All two-photon imaging experiments were carried out at RT. Two-photon imaging was performed in secondary dendrites from the distal part of the main apical dendrite of CA1 pyramidal neurons using confocal laser scanning system (Nikon Ti-E; Confocal Head A1 MP) with a 60x oil-immersion objective lens. All analyses were performed by using Nikon Ti-E software as previously described [29].

Patch-clamp analyses

Whole-cell patch-clamp recordings were obtained using a Digidata 1440 A Series interface and pClamp 10 software (Molecular Devices). Signals were filtered at 1 kHz, digitized at 10 kHz, and analyzed offline using pClamp 10. The patch-clamp electrodes were filled with internal solution containing (in mM): 135 $CsMeSO_3$, 8 NaCl, 10 HEPES, 0.25 EGTA, 2 Mg_2ATP, 0.3 Na_3GTP, 0.1 spermine, 7 phosphocreatine, and 5 QX-314, with a pH of 7.4 and an osmolarity of 310 mOsm. The extracellular solution (pH 7.4) contained (in mM): 124 NaCl, 3.2 KCl, 1.2 NaH_2PO, 10 Glucose, 23.8 $NaHCO_3$, 2 $CaCl_2$, 1 $MgCl_2$. Neurons were voltage-clamped at − 70 mV and spontaneous excitatory post-synaptic currents (sEPSC) were recorded for 3 min. For sEPSC frequency and amplitude analysis, a detection template was generated using the "Event Detection/Create Template" function, as described in [41]. Results were manually inspected to eliminate false sEPSC.

Statistical analyses

Statistical analyses were conducted using GraphPad Prism v8.4.2. The Shapiro-Wilk test was used to assess data for a normal distribution. Appropriate statistical tests were applied based on the experimental design: unpaired Student's t-test, one-sample t-test, and one-way ANOVA followed by Dunnett's multiple comparisons test were used where applicable. Two-way ANOVA followed by Sidak's post-hoc test was employed for multifactorial comparisons. The data are presented as the mean ± standard error of the mean (SEM) of independent experiments (n). Statistical significance was set at $p < 0.05$. Details (p-values, n, etc.) are provided within the text and figure legends.

Results

Complement protein levels increase in HSV-1-infected neuronal cells

Proteins of the complement system are reported to be expressed by neurons under different stress conditions, including those elicited by pathogen infections [42, 43]. Thus, to investigate whether HSV-1 affects the expression of complement proteins in rat primary neuron cultures, we infected cells at 1 and 3 MOI and assessed their complement protein content 24 h post-infection (p.i.). Mock-infected cultures served as controls (ctr). Results from western blot (WB) analyses revealed that HSV-1 infection triggered a MOI-dependent increase in the expression of a band recognized by the anti-C1q antibody ($p = 0.0339$, 3 MOI vs. 1 MOI), whose levels were almost undetectable in mock-infected cells. This band was also detected in lysates of murine liver and spleen, that we exploited as positive source controls for C1q detection (Fig. S1A). HSV-1 infection also upregulated C3 protein expression, particularly at 3 MOI ($p = 0.0303$ vs. ctr) (Fig. 1A and Fig. S1B). Therefore, we chose to perform HSV-1 infection at 3 MOI in all subsequent experiments. Confocal IF analyses of HSV-1- and mock-infected cells confirmed that the virus infection induced a significant increase of C1q ($p < 0.0001$ vs. ctr, Fig. 1B, images b vs. a) and C3 ($p = 0.0379$ vs. ctr, Fig. 1B, images d vs. c). In addition, results from RT-PCR revealed that HSV-1 infection significantly upregulated C1q and C3 mRNA levels ($p = 0.037$ and $p = 0.0038$ vs. ctr, respectively, Fig. 1C). Interestingly, HSV-1 infection also triggered a significant release of C3 protein in the culture medium, as demonstrated by ELISA results ($p = 0.0325$ vs. ctr, Fig. 1D). Our in vitro experimental model is enriched in primary neurons, but it also contains glial cells, which are the main cells expressing complement proteins in the brain. Notably, IF experiments demonstrated double labelling for C1q and NeuN (that is a marker of mature neurons) in our primary cultures (Fig. S1C) and WB of HSV-1-infected human neuroblastoma SH-SY5Y cells showed significantly higher C1q levels than mock-infected cells (Fig. S1D), thus suggesting a potential contribution also by HSV-1-infected neuronal cells, even though glia cells are the main producers of complement proteins within the brain. Overall, these data indicate that HSV-1 infection may trigger complement cascade activation in primary mixed neuron and glia cultures.

Synaptosomes are enriched of C1q and engulfed by microglia cells following HSV-1 infection

Next, on the basis of scientific literature highlighting the role of the complement system in synaptic loss observed during CNS development and in several neurodegenerative diseases [4, 10], we investigated if the HSV-1-induced increase in complement proteins was associated with their localization at synapses. To address this hypothesis, we isolated synaptosomes from HSV-1- and mock-infected primary neuron cultures 24 h p.i. and analyzed their content by WB. Specifically, we isolated the crude synaptosomal fraction (P2), that is reported to be enriched of functionally active synaptosomes [44]: we firstly compared the presence of selected markers in both P2 and nuclear (P1) fractions, as well as in total cell lysates. Results in Fig. S2A confirmed that P2 fraction

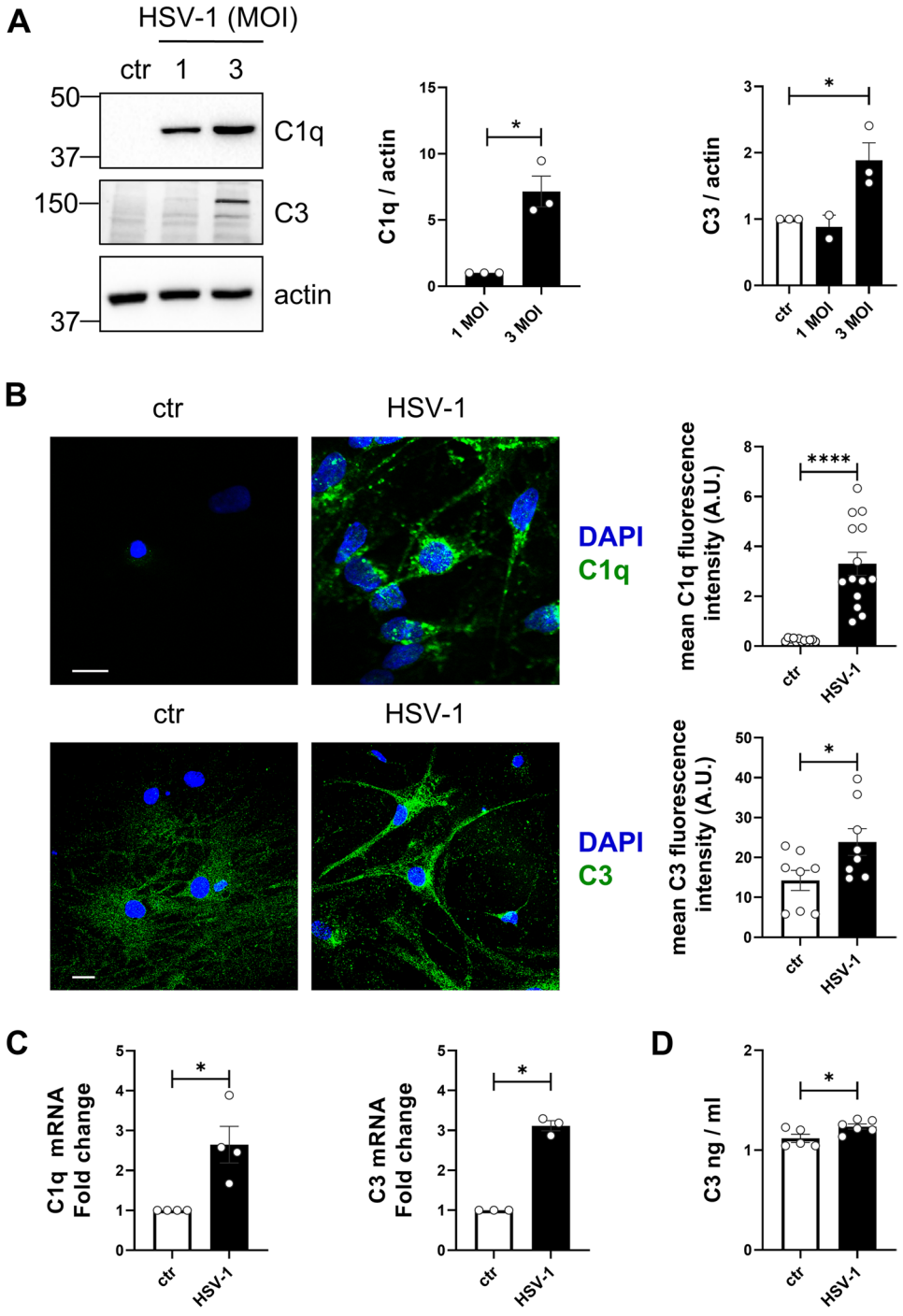

Fig. 1 HSV-1 infection triggers an increase in C1q, and C3 expression levels in rat primary neuron cultures. **A** WB analyses of C1q, and C3 expression in primary cultures of rat cortical neurons 24 h after infection with the indicated MOI of HSV-1 or mock solution inoculation (ctr). Actin expression levels were used as sample loading control. Representative WBs are shown. Densitometric analyses of $n = 3$ independent experiments are shown in the graphs, and expressed as fold changes in protein levels from HSV-1-infected cultures normalized to 1 MOI for C1q (set at 1, one-sample t-test) or to ctr (set at 1) for C3, (one-way ANOVA, followed by Dunnett's post hoc multiple comparisons). **B** Confocal immunofluorescence analyses of C1q and C3 immunoreactivity in mock- (ctr) and 3 MOI HSV-1-infected primary neuronal cultures (HSV-1) 24 h p.i. Cells were labelled with anti-C1q or anti-C3 antibodies (green) and nuclei were stained with DAPI (blue). Images show representative immunostaining (scale bars: 15 µm), whereas graphs show the mean fluorescence intensity signals of C1q and C3 immunoreactivity for 3 MOI HSV-1-infected and mock-infected cultures ($n = 2$), expressed in arbitrary units (A.U.), (unpaired t test). **C** Real-time PCR analysis showing the expression of C1q or C3 mRNA in primary neuron cultures undergoing mock- and 3 MOI HSV-1 infection for 24 h. The C1q or C3 mRNA levels were normalized to actin mRNA and are expressed as fold changes ($2^{-\Delta\Delta Ct}$) versus ctr ($n = 4$ for C1q, $n = 3$ for C3, one-sample t-test). **D** Results from ELISA assessing C3 levels in the supernatants harvested 24 h after mock (ctr) and HSV-1 infection at 3 MOI ($n = 6$, unpaired t-test). For all the experiments, data are expressed as mean ± SEM, *$p < 0.05$, ****$p < 0.0001$

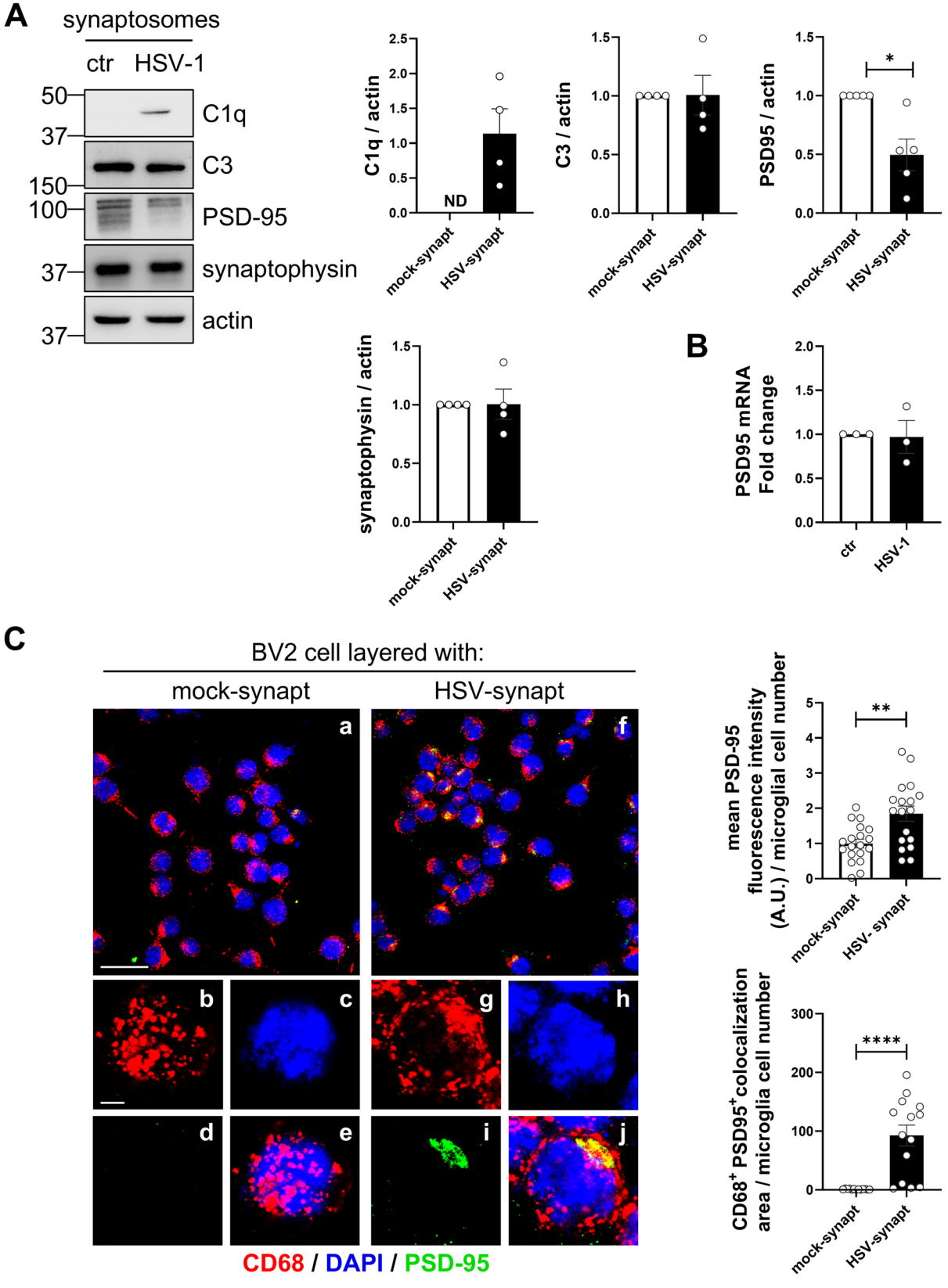

Fig. 2 (See legend on next page.)

(See figure on previous page.)

Fig. 2 HSV-1 infection triggers the presence of complement proteins at synaptosomes and increases their microglial phagocytosis. **A** WB analyses of complement C1q and C3 proteins, PSD-95, and synaptophysin in synaptosomes isolated from rat primary neuronal cultures 24 h after HSV-1 infection at 3 MOI or mock inoculation (ctr). Actin expression levels were used as a loading control. Representative blots are shown on the left. Densitometric analyses of at least $n = 4$ independent experiments are shown in the graphs on the right, and expressed as fold changes in protein levels in synaptosomes isolated from HSV-1-infected cultures (HSV-synapt) normalized to synaptosomes isolated from ctr (mock-synapt, set at 1) for the indicated proteins (one-sample t-test). Since C1q protein was not detectable (ND) in synaptosomes from mock-inoculated control cultures, C1q quantification is reported as the C1q/actin ratio found in HSV-1-synapt. **B** Real-time PCR analysis showing the expression of PSD-95 mRNA in total cell lysates of primary cultures undergone mock (ctr) and 3 MOI HSV-1 infection for 24 h. The PSD-95 mRNA levels were normalized to actin mRNA and are expressed as fold changes ($2^{-\Delta\Delta Ct}$) versus ctr (one-sample t-test). **C** Confocal immunofluorescence analyses of the engulfment assay showing CD68 (red) and PSD-95 (green) immunofluorescence (nuclei were stained in blue with DAPI). (a-j) Representative images showing BV2 layered with synaptosomes isolated from primary cultures of mouse neurons 24 h after either mock (a-e) or 3 MOI HSV-1 infection (f-j). Scale bars: 30 µm for a and f images and 10 µm for b-e and g-j images. The top graph on the right shows the mean fluorescence intensity of PSD-95 signals, expressed as arbitrary units (A.U.) and further normalized for the number of microglial cells/field; the bottom graph on the right shows colocalization area of CD68 and PSD-95 signals normalized to the number of $CD68^+$ cells/field. At least 4–6 fields/group for each experiment were analyzed ($n = 3$, unpaired t-test). For all the experiments, data are expressed as mean ± SEM, $^*p < 0.05$, $^{**}p < 0.01$, $^{****}p < 0.0001$

was enriched of the synaptic PSD-95 protein, whereas P1 was enriched of the nuclear marker SMC-3.

We then checked P2 obtained from HSV-1 and mock-infected cultures for the presence of complement proteins as well as of synaptic markers. We detected C1q in the P2 fraction isolated from HSV-1-infected cultures, whereas this protein was almost undetectable in the one isolated from mock-infected cells (Fig. 2A). On the contrary, C3 was also found in P2 isolated from mock-infected cultures and it was unaffected by virus infection (Fig. 2A). Overall, these data indicate increased amounts of C1q at the synapses of HSV-1-infected cells, suggesting that this protein could represent a tag for those synapses to be eliminated. Upon virus infection, we also found a significant decrease in the expression of the post-synaptic marker PSD-95, whereas its mRNA in total cell lysates was unchanged (Fig. 2A and B, $p = 0.0202$ and $p = 0.8804$ vs. ctr, respectively). On the contrary, we did not find significant changes in the expression of the pre-synaptic protein synaptophysin in synaptosomes from HSV-1-infected rat primary neurons. Thus, we selected PSD-95 protein to investigate the HSV-1-driven synaptic alteration in the following experiments.

To verify if the presence of complement proteins at synaptic levels represents a tag for microglia-mediated synapse ingestion, we set up an engulfment assay. For this and the following experiments involving microglia cells, we used the mouse microglial BV2 cell line and mouse primary neurons as neuronal counterparts. Specifically, we first isolated P2-synaptosomes from primary cultures of mouse neurons 24 h after mock and HSV-1 infection at 3 MOI and provided additional characterization of the synaptosome preparation for PSD-95 and synaptophysin expression by IF. Synaptosome staining for either PSD-95 or synaptophysin (Fig. S2B, C) revealed fluorescent spots with a diameter consistent with the synaptosome size [45]. We then layered the synaptosome preparation onto BV2 microglial cells and analyzed their possible ingestion by BV2 2 h later by IF staining for the microglial lysosomal marker CD68 and PSD-95. Specifically, on the basis of the HSV-1-driven PSD-95 downregulation at synaptosome (Fig. 2A), we selected this post-synaptic protein to investigate the HSV-1-driven synaptic alteration in this and the following experiments.

Interestingly, IF analyses of synaptosome-layered BV2 cells (Fig. 2C) revealed that green spots (detecting PSD-95) were mainly found in BV2 layered with synaptosomes from HSV-1-infected neurons (HSV-synapt) with respect to mock-infected ones (mock-synapt) (Fig. 2C, upper graph). In addition, PSD-95 signals colocalized with red signals (detecting $CD68^+$ microglial lysosomes) mainly in BV2 cells layered with HSV-synap (Fig. 2C, lower graph).

Overall, these results suggest that HSV-synapt underwent a higher uptake by BV2 cells than mock-synapt.

HSV-1 infection induces complement-dependent microglial synaptic pruning in primary neurons supplemented with microglial cells

To confirm the results from the engulfment assay, we next checked whether HSV-1 infection triggers microglia-mediated synaptic pruning in a more complex cellular context, and if complement inhibition prevents this effect. For these experiments, we used mouse primary neurons co-cultured with mouse microglial cells as experimental model of infection (see experimental flow chart in Fig. 3A). According to the previous experiments, we infected co-cultures with 3 MOI HSV-1 for 24 h: under these experimental conditions, a slight cytopathic effect induced by the viral infection was observed, whereas cellular integrity was preserved for subsequent analyses (Fig. S3A, B). As we reported the occurrence of neuroinflammation and neurotoxic M1-like activation of microglia upon virus replication in mice [25, 27] and Li Puma et al., Neural Regen Res 2026 (in press), we first evaluated if HSV-1 induced a similar trend in our in vitro neuron-BV2 co-cultures. RT-PCR analyses showed that HSV-1 induced the transcriptional upregulation of IL-1β, interleukin-6 (IL-6) and inducible nitric oxide synthase (iNOS) genes 24 h p.i., paralleled by the expected mRNA downregulation of the Arginase 1 gene (Arg1),

as this gene is negatively correlated with the expression of iNOS (Fig. 3B). Of note, we also detected a significant transcriptional upregulation of interleukin-10 (IL-10) gene, whereas CD206 mRNA was unaffected by the viral infection. Altogether these findings suggest that HSV-1 induces a heterogeneous activation of microglia, mainly polarized toward a pro-inflammatory M1-like phenotype, that is reportedly involved in synaptic pruning as reviewed in Zhao et al, 2025 [46]. We thus investigated the possible pruning of post-synaptic terminals upon HSV-1 infection and the role of C3 protein in this process, since it is the effector of the complement-dependent synapse opsonization [3, 14]. To this aim, IF experiments were performed to check whether, upon 24 h of HSV-1 infection, synapses labelled for PSD-95 presence were found inside microglia, identified by expression of the lysosomal marker CD68, classically considered as a marker of 'activated' phagocytic microglia [47]. To investigate the role of C3 protein, HSV-1 infection was performed in the presence or absence of an anti-C3 antibody (C3 Ab), which binds C3 thus inhibiting complement cascade activation, and a matched isotype immunoglobulin as control (IgG). Figure 3C, D shows that the virus infection induced a significant increase in the area of colocalization between PSD-95 immunoreactive signals and $CD68^+$ lysosomes, indicated by white spots (see panels h vs d; $p < 0.0001$ vs ctr). Interestingly, such colocalization was significantly lower ($p = 0.0007$, HSV-1 + C3 Ab vs HSV-1) when the co-cultures were infected in the presence of C3 Ab (see panels p vs h in Fig. 3D), whereas it was unaffected by control IgG treatment (panels y vs h). Of note, either C3 Ab or control IgG treatments did not affect cell viability as well as the efficacy of the infection, as indicated by results from MTT assay and SPA shown in Fig. S3C, D.

In addition, we observed two distinct shapes of microglia immunostained by the anti-CD68 antibody. Both rounded- and oblong/ameboid-like microglia (see white arrows in Fig. S3E) were present in all the experimental groups, but a significant increase in the latter morphology of $CD68^+$ cells appeared (Fig. S3E, $p < 0.0001$ HSV-1 vs. ctr) after HSV-1 infection. These changes were rescued by the C3 Ab treatment ($p < 0.0001$ HSV-1 vs. HSV-1 + C3 Ab), whereas were unaffected by control IgG one. Notably, both forms appeared to be involved in the virus-induced synaptic pruning (Fig. 3C, see panel h). In addition, we checked whether microglia reduced viral replication in neurons under co-culture conditions, comparing viral titer in supernatants from HSV-1-infected primary neurons supplemented or not with BV-2 cells. Results reported in Fig. S3D show that, under our experimental conditions (i.e., neuron/microglia = 5/1 ratio, 24 h p.i.) BV2 cells do not contribute to viral clearance since we found similar amount of viral titer in the two experimental model supernatants.

Furthermore, as expected, we also found that virus infection significantly affected the expression levels of PSD-95 in co-cultures 24 h p.i., confirming results previously reported by our group in other in vitro and in vivo mouse models of infection [24, 27]. Conversely, in co-cultures treated with C3 Ab, HSV-1 failed to significantly reduce PSD-95 expression (Fig. S4A).

Overall, these results suggest that HSV-1 triggers a post-synaptic pruning by microglial cells and that C3 is involved in this process.

HSV-1 induces microglial pruning of synaptic material and alterations of synaptic transmission in organotypic hippocampal slices

Next, we investigated the HSV-1-triggered microglial synaptic pruning in an ex-vivo model of mouse brain. To this aim, we first biolistically transfected organotypic hippocampal slices from P7 mice with the EGFP plasmid to sparsely label a limited number of neurons within each slice, facilitating high-contrast visualization of neuronal structures (e.g., dendrites and spines) without overlaps from neighboring ones. Two days after transfection, slices bearing fluorescent CA1 neurons were infected with 1×10^5 PFU of HSV-1 and analyzed 48 h later. In Fig. S5B, representative confocal images of transfected organotypic hippocampal slices with EGFP-expressing cells (green) following 48 h of mock (ctr) or HSV-1 infection are shown, indicating that the virus infection did not affect the expression of fluorescent EGFP. First, we assessed the efficacy of HSV-1 infection by evaluating the expression of the viral glycoprotein gB in hippocampal slices by IF and WB (Fig. 4A and B). Furthermore, our results confirmed that HSV-1 affected synaptic marker expression in this model of infection, since we found a significant decrease in PSD-95 expression following virus infection (Fig. 4B, $p = 0.046$ vs. ctr). Then, we analyzed the EGFP-transfected hippocampal slices to check the occurrence of HSV-1-driven microglial phagocytosis of EGFP-fluorescent neurons. To this aim, we stained the organotypic hippocampal slices with anti-CD68 antibody and studied them by IF (Fig. 4C). Using Z-stacks, we analyzed the three-dimensional volume of green-fluorescent neuronal material (inside microglial lysosomes stained with anti-CD68 antibody (red) by quantifying the colocalized signals. We found that microglial cells in HSV-1-infected EGFP-expressing organotypic hippocampal slices were engulfed of a higher amount of neuronal material (Fig. 4C) with respect to mock-infected ones ($p = 0.013$ vs. ctr). More details are given in Additional file 1–4. These data suggest an HSV-1-triggered microglial pruning of neuronal material (likely synaptic) also in mouse hippocampal organotypic slices. Notably,

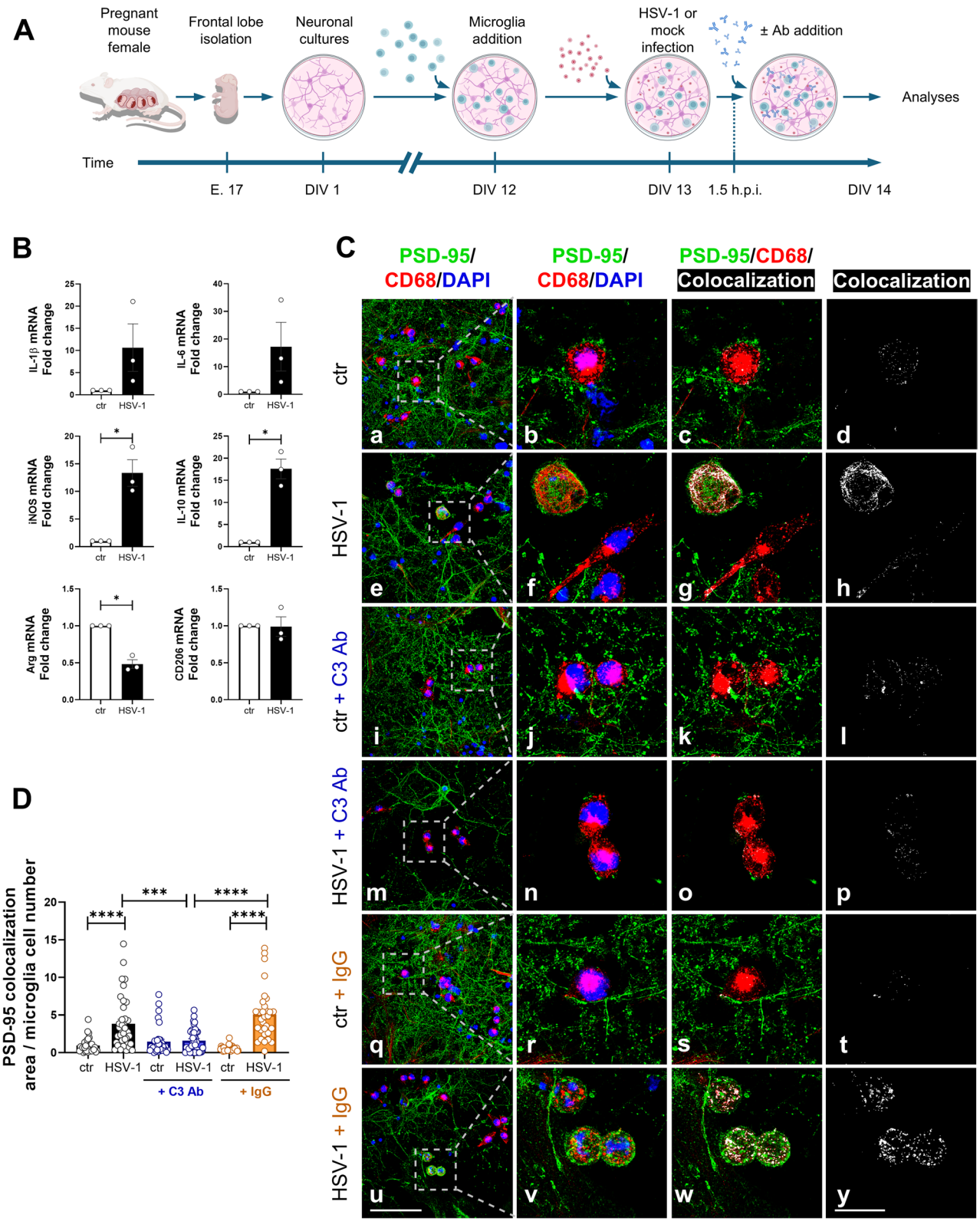

Fig. 3 (See legend on next page.)

(See figure on previous page.)

Fig. 3 HSV-1 infection induces complement-dependent microglial post-synaptic pruning in mouse primary neurons supplemented with microglial cells. **A** Experimental design flow-chart: frontal lobes were isolated from E17 mouse embryos and dissociated to isolate primary neurons. After 12 days of culture in vitro (DIV 12), neuronal cultures were supplemented with microglia to obtain neuronal-microglia co-cultures. Twenty-four h later (DIV13) co-cultures were inoculated with 3 MOI HSV-1 or mock solution. After 1.5 h of virus adsorption, the infection medium was discarded, co-cultures were gently washed with PBS and then cultured with DIV 13-conditioned medium for additional 24 h. For complement inhibition experiments, DIV 13-conditioned medium was supplemented with 1 µg/ml of C3 Ab or control IgG. Cells and supernatants were collected at DIV 14 for downstream analyses. The flow-chart was created using BioRender (https://biorender.com). **B** Real-time PCR analyses showing the expression of IL-1β, IL-6, iNOS, IL-10, Arg1 and CD206 mRNA in co-cultures of primary neuron and BV2 cells undergone mock or 3 MOI HSV-1 infection for 24 h. The indicated gene mRNA levels were normalized to the appropriate housekeeping gene (GAPDH for CD206 and actin for the other genes) and are expressed as fold changes ($2^{-\Delta\Delta Ct}$) versus ctr ($n = 3$, one-sample t-test). **C**, **D** Confocal immunofluorescence of mock- and HSV-1-infected co-cultures of mouse primary neurons and microglial cells and treated or not with C3 Ab (1 µg/ml) or matched isotype control immunoglobulin (IgG) within 24 h of infection. Fixed cells were labeled with anti-CD68 (red) and anti-PSD-95 (green signals) antibodies, and nuclei were stained with DAPI (blue). Images of a representative experiment are shown: left column images were acquired with 40x magnification oil-immersion objective (scale bar: 50 µm) and higher magnification (40x objective, zoom 3) of boxes outlined in each panel are shown in the other three columns (scale bar: 20 µm). The graph in D shows results from PSD-95 and CD68 colocalization area normalized to the number of $CD68^+$ cells in the indicated conditions ($n = 3$, 5–9 field/group for each experiment, two-way ANOVA, followed by the Sidak post-hoc test. $^*p < 0.05$, $^{***}p < 0.001$ and $^{****}p < 0.0001$)

treatment with C3 Ab appeared to prevent this event, since significant decreased amounts of green-fluorescent spots were found in C3 Ab-treated HSV-1-infected slices compared to untreated-infected brain slices ($p = 0.0034$ HSV vs. HSV + C3 Ab). Next, in two-photon live imaging experiments, we examined dendritic spine density of EGFP-transfected CA1 neurons in organotypic hippocampal slices undergoing HSV-1 or mock infection in the presence or absence of C3 Ab. Our analysis revealed a significant decrease in dendritic spine density in neurons infected with HSV-1 compared to mock-infected controls ($p = 0.0004$; Fig. 5A, B), supporting the occurrence of HSV-1-induced synaptic pruning. Importantly, the observed reduction in spine density was effectively reversed when HSV-1 infection was conducted in the presence of the C3 Ab, demonstrating that the blockade of C3 mitigates the HSV-1-induced alterations in dendritic spine density ($p = 0.0031$ HSV-1 vs. HSV-1 + C3 Ab).

Finally, to assess whether the HSV-1-induced reduction in dendritic spine density was paralleled by functional alterations in synaptic transmission, we performed whole-cell patch-clamp recordings in CA1 pyramidal neurons from organotypic hippocampal slices undergone 48 h of HSV-1 infection in the presence or absence of C3 Ab. Specifically, we recorded spontaneous excitatory postsynaptic currents (sEPSCs) and quantitative analysis revealed a significant increase in sEPSC frequency in HSV-1-infected slices compared to mock-infected controls (Fig. 5C, D, left graph). This HSV-1-mediated increase in sEPSC frequency was significantly reduced by treatment with the C3 Ab, resulting in values comparable to mock-treated slices. In contrast, sEPSC amplitude did not differ significantly among mock, HSV-1–infected, and C3 Ab-treated HSV-1 slices (Fig. 5D, right graph). In a subset of experiments, virus infections were also performed in the presence of control IgG, used as a matched control for the C3 Ab treatment. In the presence of IgG, HSV-1-mediated synaptic alterations were still evident, indicating that control IgG did not prevent the synaptic effects induced by HSV1 (Fig. S4C, D).

Altogether, these data indicate that HSV-1 infection induces early complement-dependent alterations in excitatory synaptic activity in organotypic hippocampal slices.

Discussion

Although a growing body of evidence supports the role of recurrent HSV-1 infection in driving synaptic dysfunction reminiscent of AD, the molecular mechanisms underlying the virus-induced brain damage are not fully clarified. The present study provides evidence of a novel mechanism that may underlie the HSV-1-induced synaptic damage in murine primary neuronal cells and brain tissues. Indeed, we demonstrated that HSV-1 infection in cultured neurons and hippocampal brain slices triggers the upregulation of key components of the complement cascade that cooperate with microglia for the phagocytosis of the synapses damaged by the virus.

Most studies reporting a possible link between complement activation and HSV-1 infection are very dated, especially those related to in vitro models of infection in epithelial cells [48, 49]. Such studies suggest an interaction between the virus and complement cascade proteins, particularly highlighting the ability of the virus to evade cellular mechanisms related to complement-dependent innate immunity. Other studies reported a key role of the complement cascade in the immune response to the virus, evidencing that C4- and C3-deficient mice failed to generate a normal memory response against HSV-1 compared to wild-type (WT) [50]. Moreover, mouse deficits in the complement lectin pathway showed higher mortality compared to WT in the context of HSE [51]. Interestingly, increased levels of complement proteins were found in the CSF of subjects affected by HSE compared to healthy subjects, indicating that the complement system is activated within active HSV-1 replication in the

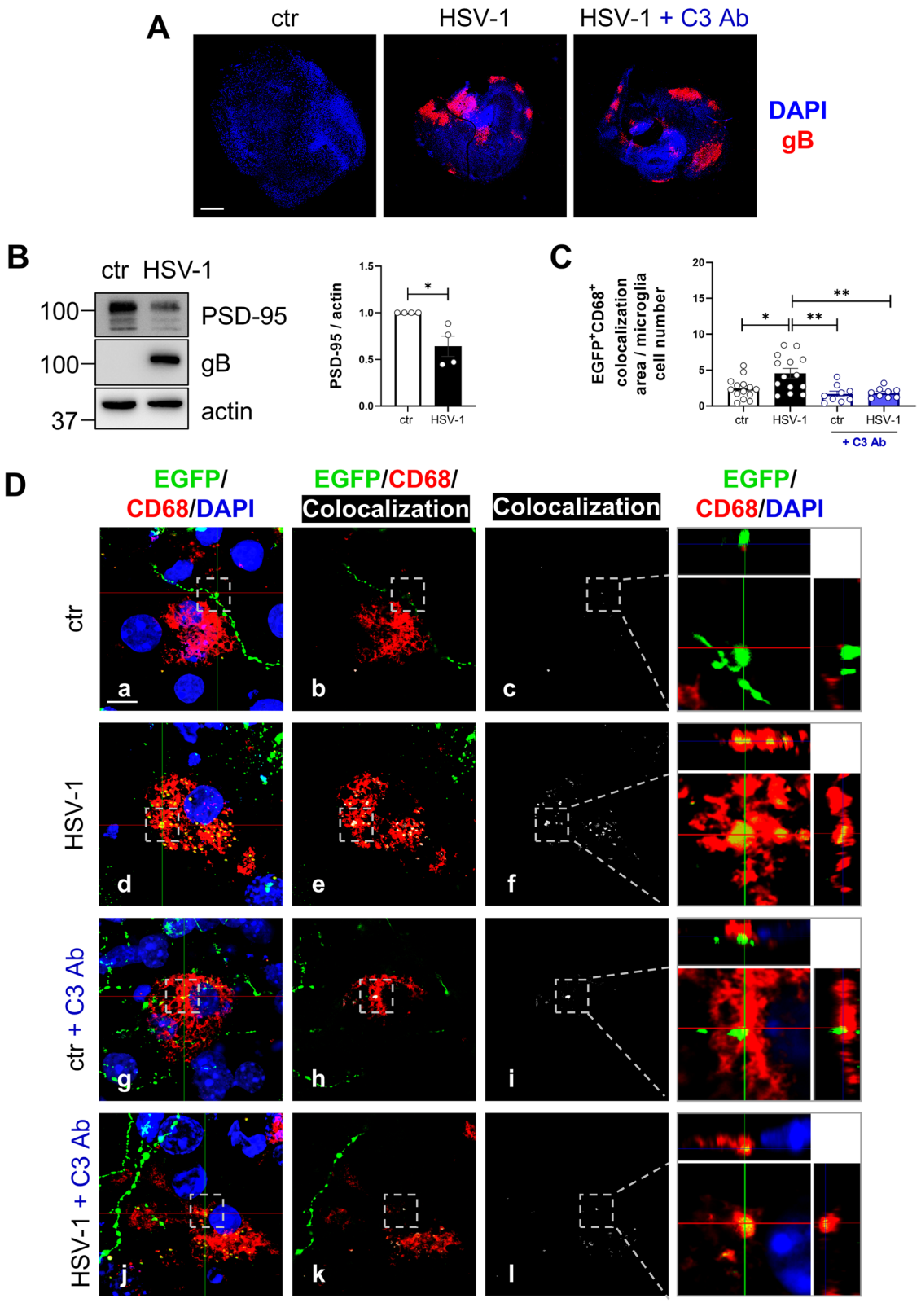

Fig. 4 (See legend on next page.)

(See figure on previous page.)

Fig. 4 HSV-1 induces microglial pruning of synaptic material in mouse organotypic hippocampal slices. **A** Confocal immunofluorescence analyses of mock- and HSV-1-infected (1×10^5 PFU) mouse organotypic hippocampal slices in the presence or absence of C3 Ab. Forty-eight h p.i., slices were fixed and labeled with anti-gB antibody (red) and DAPI for nuclei detection (blue). Representative images are shown, scale bars: 300 µm. **B** WB analyses of PSD-95, and gB expression 48 h after HSV-1 infection. Actin detection was used as sample loading control. Representative blots are shown on the left. Normalized densitometric analysis of PSD-95 signals in $n = 4$ independent experiments are shown in the graph on the right as the fold changes in protein levels from HSV-1 normalized to ctr (set at 1, one-sample t-test). **C, D** 3D Confocal immunofluorescence analyses of mock- and HSV-1-infected mouse hippocampal organotypic slices transfected with EGFP neuronal fluorescence (green) and treated or not with C3 Ab. Slices were fixed 48 h after infection and labelled with anti-CD68 antibody (red) and DAPI (blue) for nuclei staining. In C, first column on the left shows representative maximum projections of 3D confocal images for each experimental group. Second column shows one representative plane of the z-stack where the colocalization of CD68 and EGFP neuronal fluorescence is shown in white. Colocalization channel alone is showed in the third column as a representative colocalization map that was quantified. The right column shows higher magnification of dashed boxes for each condition: XZ and YZ orthogonal views were sliced at the indicated intersections (green/red lines), revealing the colocalized signal (yellow) inside the microglial lysosomes marked by CD68 immunostaining. Analyses were performed in at least 62 cells/group (9–14 fields/group. Scale bars: 10 µm. Significant differences were assessed by two-way ANOVA with Sidak post-hoc multiple comparisons. For all the experiments, data are expressed as mean ± SEM, $*p < 0.05$, $**p < 0.01$

human brain, likely contributing to neuroinflammation and brain damage [52].

Here, we report that HSV-1 infection increases complement proteins C1q and C3 in murine primary neuronal cultures (Fig. 1), which consist of neurons and glial cells. Although glial cells are the primary source of complement protein expression and release in the brain, neurons may also contribute to their production, especially within specific steps of brain development and following different injuries [6, 53–57]. We also show that HSV-1 infection triggers C1q upregulation in SH-SY5Y human neuroblastoma cells (Fig. S1D), thus supporting the idea that the increase in C1q in HSV-1-infected murine primary cultures may also result from a neuronal contribution, as previously reported for SH-SY5Y cells [46, 48], along with a massive production by glia [54, 58]. Interestingly, we observed the virus-induced complement protein upregulation both at mRNA and protein levels, indicating that the virus triggers the activation of the complement cascade (Fig. 1).

Notably, we found that HSV-1 triggers C1q localization at synaptosomes (Fig. 2A), which are subcellular components isolated from nerve endings, commonly exploited for studies regarding the synaptic structure and function [44, 59]: this result suggests that C1q may play a role at synaptic level, as that elicited for synaptic pruning [4]. We also found that HSV-1 infection induced a decrease of the post-synaptic marker PSD-95 in synaptosomes isolated from primary neurons (Fig. 2A), as well as in total neuronal lysates (Fig. S4D) and in hippocampal brain slices (Fig. 4B). Such a decrease in protein levels was not due to a possible virus-induced shut-off of the PSD-95 gene, as our results from RT-PCR analyses showed no difference in PSD-95 mRNA after HSV-1 infection at 3 MOI (Fig. 2B). Hence, our data further support previous results by our group demonstrating the HSV-1-induced synaptic damage [24, 27] and suggest a possible involvement of complement proteins. On the contrary, we did not find decreased levels of synaptophysin at synaptosomes derived from HSV-1-infected cells compared to controls, suggesting that under our experimental conditions (e.g., 24 h of 3 MOI HSV-1 infection in an in vitro model of rat cortical neurons), the virus primarily affects post-synaptic termini, whereas we already provided in vivo evidence that recurrent HSV-1 infection affects both pre- and post-synaptic termini in mouse brain [27]. However, such a hypothesis requires additional experiments to be supported and would warrant a dedicated study.

We thus investigated if the virus-induced complement enrichment at synaptosomal level may elicit "eat me" signals that can be recognized and used by microglial cells for targeted synaptic or neuronal elimination [10, 60]. The engulfment assay we set up confirmed the capacity of BV2 cells to make contact with synaptic material, particularly from HSV-1-infected cultures: we indeed found that BV2 cells interact with a higher amount of synaptosomes isolated from HSV-1-infected cultures compared to mock-infected ones (Fig. 2C). Consistently, results from our analyses in IF, which is a gold standard imaging method to study phagocytic activity and synaptic pruning [61], revealed that these events increased following HSV-1 infection of the murine neuronal cultures supplemented with the microglial BV2 cells. Indeed, these results revealed higher colocalization of PSD-95 signals with CD68-labeled microglial cells upon virus infection, indicating that the virus elicits a microglia-mediated synaptic pruning, which was inhibited by C3 Ab, but not by a control IgG (Fig. 3C). Of note, neither C3 Ab nor IgG treatments affect both virus replication and cell viability, thus confirming the specific involvement of complement cascade activation in HSV-1-induced synaptic alterations. Similar results were found in organotypic hippocampal brain slices, which better recapitulate the complex cytoarchitecture of the brain, as we detected following 48 h of HSV-1 infection an increased microglial engulfment of neuronal material, likely synaptic one, that was rescued by C3 Ab treatment (Fig. 4). Indeed, herein we also found that HSV-1 induces a significant decrease in spine density that was recovered upon C3 Ab treatment (Fig. 5). Furthermore, these events were accompanied by changes in synaptic transmission, as we recorded a significant increase in sEPSCs in HSV-1-infected slices

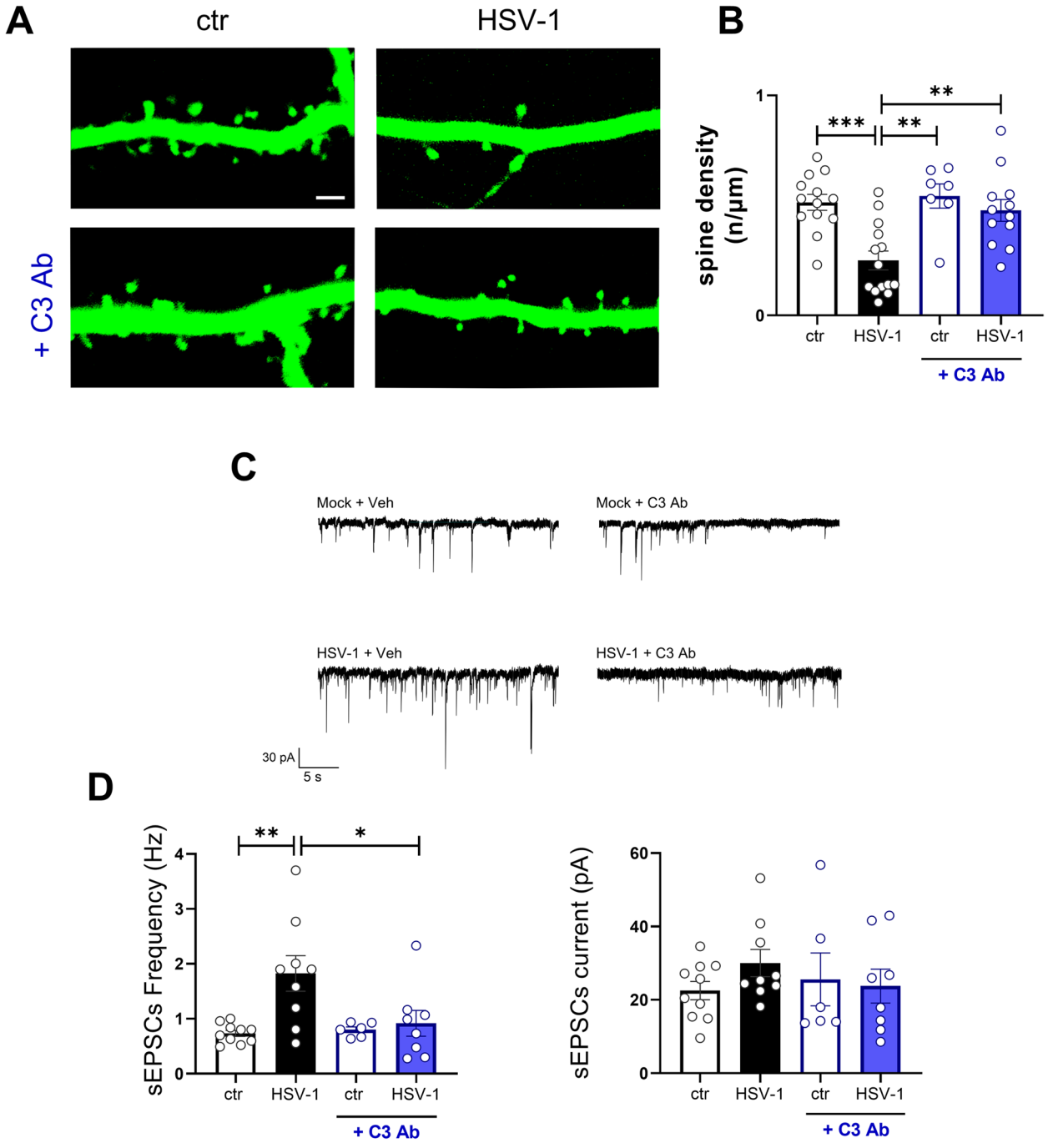

Fig. 5 HSV-1 triggers spine density decrease and synaptic alterations in a complement-dependent manner. Two-photon analyses of dendritic spine density in EGFP-transfected organotypic brain slices following 48 h of HSV-1 or mock- infection (ctr) in the presence or absence of C3 Ab. Representative two-photon images in dendrites of EGFP-transfected CA1 neurons are shown in (**A**). Scale bars, 2 µm. (**B**) Quantification of dendritic spine density (spine number/µm). **C** Representative traces of spontaneous excitatory post-synaptic currents (sEPSCs) recorded in CA1 neurons from organotypic hippocampal slice cultures undergone 48 h of mock- (ctr) or HSV-1- infection in the absence or presence of C3 Ab. Scale bars: 30 pA, 5 s. **D** Bar graphs showing the mean sEPSC frequency (left) and sEPSC amplitude (right) recorded in neurons from ctr and HSV-1-infected organotypic hippocampal slice cultures under the indicated conditions. Significant differences were assessed by two-way ANOVA with Sidak post-hoc multiple comparisons and are indicated by $*p < 0.05$, $**p < 0.01$, $***p < 0.001$. Data are mean ± SEM from technical replicates of $n = 3$ independent organotypic slice preparation

relative to mock controls (Fig. 5C, D). We previously reported that HSV-1-infected neurons display increased intrinsic excitability due to the inhibition of leak potassium currents and the selective activation of persistent sodium currents [62]. This effect may explain the increased frequency of sEPSCs we observed here even in the presence of reduced dendritic spine number. Indeed, since in our experimental set up we did not use the tetrodotoxin toxin to block voltage-gated sodium channel, we collected data from organotypic hippocampal slices where the neighboring cells of the recorded neurons are embedded in an intact functional network and are capable of generating and propagating action potentials. Conversely, in another study from our laboratory, in which synaptic function was assessed in voltage-clamped single autaptic neurons, preventing action potential firing, HSV-1 infection induced instead a decrease in frequency of miniature EPSCs [24].

Altogether, our data suggest that HSV-1 infection triggers aberrant complement activation and microglial engulfment of damaged synapses, possibly driven by the complement-tag, in primary brain cultures, which result in structural synaptic deficits and alterations in excitatory synaptic signaling.

It is known that reactive microglia trigger A1 reactive astrocytes through the secretion of inflammatory mediators, including IL-1α, TNFα, and C1q [63]. Moreover, astrocytes in a reactive state are capable of participating in synapse elimination through the MEGF10 and MERTK phagocytic pathways [64]. Considering the HSV-1-induced C1q increase we found in primary cultures of neurons, that also contain astrocytes, we cannot exclude the involvement of these glial cells in HSV-1-induced synaptic pruning. Interestingly, our group previously reported the occurrence of astrogliosis, an evident sign of reactive astrocytes, following recurrent HSV-1 infection reaching the brain [25]. In addition, as recently reported by Deivasigamani and co-workers, complement-mediated microglia phagocytosis may also target the whole neuron cell body [60]. Interestingly, HSV-1 infection has been shown to induce microglial activation in the brains of 5xFAD transgenic mice, leading to the phagocytosis of infected neurons. However, the authors did not examine whether complement signaling is implicated in such process [65]. Further studies are warranted to assess whether complement activation contributes to microglial engulfment of whole neurons in the context of HSV-1-induced neuroinflammation.

Complement is traditionally known as a serum-effective system, but novel insights into complement biology have identified cell-autonomous and intracellularly active complement -the complosome- [66]. Beyond its classical immune function, the complosome regulates mitochondrial activity, energy metabolism, and gene expression in both immune cells and fibroblasts. Emerging evidence suggests that the complosome might contribute to neuronal cell physiology, although its exact role remains to be elucidated [66]. If this is the case, the HSV-1-induced upregulation of complement proteins could potentially lead to many other pathological changes.

Interestingly, recent findings support Aβ and hyperphosphorylated tau as possible triggers for complement cascade activation in the brain [42], and several studies, including ours, showed that HSV-1 induces the accumulation of these neurotoxic proteins in neuronal cells and mouse brains [21, 22, 25, 26, 67, 68]. It is thus possible to speculate that, besides the virus itself, also the virus-induced Aβ and hyperphosphorylated tau may contribute to the activation of the complement cascade that in turn may lead to synaptic loss. Notably, Zelek et al. [69] very recently demonstrated that a brain-penetrant antibody against the terminal complement complex reduced synaptic damage and improved cognition in an AD mouse model, proposing inhibition of the complement system as a promising therapeutical approach. According to our data, this potential approach may also be effective in targeting HSV-1-induced neurodegeneration, even though the effect of the inhibition of the complement cascade within a pathogen infection should be carefullly evaluated.

Moreover, as within brain development where less active synapses must be eliminated, complement-mediated synaptic pruning may represent a protective mechanism to limit HSV-1 and/or other neurotropic virus spreading to the brain. If so, this type of immune response, initially protective, might become dysregulated or excessive, ultimately contributing to pathology rather than protection, thus supporting the dual-edged role of neuroinflammation in viral infections.

Conclusions

Overall, our findings indicate that HSV-1 infection triggers aberrant complement activation and complement-mediated microglial engulfment of damaged synapses, thus providing a novel understanding of how recurrent HSV-1 infection may contribute to synaptic loss in AD.

Supplementary Information

The online version contains supplementary material available at https://doi.org/10.1186/s12964-026-02745-y.

Supplementary Material 1: Fig. S1. Additional detection of virus-induced complement protein upregulation in primary neurons and SH-SY5Y cells. (A) Representative WB analysis of C1q protein expression in rat primary neuronal cultures (PNCs) 24 h after HSV-1 infection at 3 MOI or mock inoculation (ctr). Murine liver and spleen lysates were used as positive controls for C1q detection. Ponceau S staining is shown as a loading control. (B) Representative WB analysis of C3 protein expression in rat PNCs 24 h after HSV-1 infection at 1 and 3 MOI or mock inoculation (ctr). Murine liver lysates were used as positive controls for C3 detection. Actin detection was used as sample loading control. (C) Representative confo-

cal immunofluorescence images of C1q (green signals) and NeuN (red signals) immunoreactivity in mock (ctr) and 3 MOI HSV-1-infected primary neuronal cultures 24 h p.i.. Nuclei were stained with DAPI (blue). Scale bars: 15 µm. (D) Representative WBs of C1q and C3 protein expression levels in SH-SY5Y cell lysates harvested 24 h p.i. with 3 MOI of HSV-1 or mock-infected (ctr). Actin expression levels were used as sample loading controls. The densitometric analyses of the indicated proteins were performed with ImageJ software and normalized to actin expression level. Because C1q protein was not detectable (ND) in mock-infected SH-SY5Y cells, C1q quantification is reported in the graph as the C1q/actin ratio found in HSV-1-infected cells. For C3, the graphs represent the fold changes in protein levels from HSV-1 normalized to ctr (set at 1). Significant differences were assessed by one-sample t-test, and data are mean ± SEM from n = 3 independent experiments.

Supplementary Material 2: Fig. S2. Characterization of synaptosome isolations by WB and confocal microscopy. (A) Representative WB analysis of the indicated proteins in nuclear (P1) and synaptosomal (P2) fractions and total cell lysate (Lysate). Blots of low and high exposures of the same membrane are shown to allow visualization of both high- and low-intensity signals. SMC3 and PSD-95 were used as markers of nuclear and synaptic compartments, respectively. Actin served as a loading control. (B-C) Representative confocal images of isolated synaptosomes immunoassayed for PSD-95 (green) (B) and synaptophysin (green) (C) expression. Scale bar: 10 µm. Magnified imagines in the box for both (B) and (C) shows an example of dimension measurements in µm. Scale bar: 1 µm. Histograms show the size distribution of the analyzed synaptosomes with anti-PSD-95 (left, n =161), and anti-synaptophysin (right, n =181) antibodies staining.

Supplementary Material 3: Fig. S3 Additional experimental controls supporting data in Fig 3. (A) Representative phase-contrast microscopy images from mouse primary neuronal cultures (Mouse PNCs) 24 h after HSV-1 infection at 3 MOI or mock inoculation (ctr), in the absence or presence of microglia. Arrows indicate microglial cells in co-culture conditions. Scale bar, 100 µm. (B-C) MTT assays assessing cell viability in co-cultures of mouse primary neurons and microglia 24 h after (B) HSV-1 infection at 3 MOI or mock inoculation or (C) treatments with 1 µg/ml C3 Ab or 1 µg/ml isotype-matched control IgG, as indicated (one-simple t-test for B, one-way ANOVA, followed by Dunnett's post-hoc multiple comparison for C). (D) Results from SPA titration of virus released from Mouse PNC or from co-culture of Mouse PNC and microglia (+microglia) 24 h after infection with 3 MOI HSV-1. Where indicated, after virus absorption, cells were treated with 1 µg/ml anti-C3 antibody (+C3 Ab) or isotype IgG control (+IgG) within the 24 h of infection. Viral titers are expressed as plaque-forming units per milliliter (PFU/mL). Data represent mean ± SEM from 3 independent experiments. (E) Representative images of confocal microscopy analyses of mock- and HSV-1-infected co-cultures of mouse primary neurons and microglial cells untreated or treated with anti-C3 antibody (+C3 Ab, 1 µg/ml) or matched isotype IgG (+IgG, 1 µg/ml) within the 24 h of infection. Fixed cells were labelled with anti-CD68 antibody (red) and nuclei were stained with DAPI (blue); scale bars: 50 µm, Arrowheads indicate examples of the observed oblong/amoeboid-like cells. Bar graph shows the ratio between the number of oblong and spindle CD68+ cells and the total number of CD68+ cells. (n = 3 independent experiments, two-way ANOVA followed by the Sidak post-hoc test).

Supplementary Material 4: Fig. S4. WB analyses of PSD-95 expression in HSV-1-infected co-cultures and) and additional experiments to support data in Fig. 4 and Fig. 5 5. (A) WB analyses of PSD-95 expression 24 h post 3MOI HSV-1 infection in the presence or absence of C3 Ab (1 µg/ml). Actin detection was used as a sample loading control. A representative blot is shown on the left. Densitometric analyses of n = 3 independent experiments are shown in the graph and expressed as fold changes vs ctr (two-way ANOVA followed by the Sidak post-hoc test). (B) Organotypic slices were fixed 48 h after infection and labeled with DAPI (blue) for nuclei staining. Scale bar: 200 µm. (C) Representative traces of spontaneous excitatory post-synaptic currents (sEPSCs) recorded in neurons from organotypic hippocampal slice cultures undergone 48 h of mock- (ctr) or HSV-1- infection in the presence of IgG. Scale bars: 30 pA, 5 s. (D) Bar graphs showing the mean sEPSC frequency (left) and sEPSC amplitude (right) recorded in neurons from ctr and HSV-1–infected organotypic hippocampal slice cultures under the conditions indicated in C. Significant differences were assessed by unpaired t-test, and are indicated by * $p <$ 0.05. Data are mean ± SEM from technical replicates of n = 3 independent organotypic slices preparation.

Supplementary Material 5: Full uncropped Gels and Blots images_S1 Data shows the whole uncropped images of original WB from which Figures have been derived. When appropriate, left images show color-merged blots, right images show the corresponding original unmerged blot as presented in the figures.

Additional file 1: Video showing 3D confocal immunofluorescence analyses, reported in Fig. 4D, of mouse hippocampal organotypic slices transfected with EGFP. Video shows a representative microglial cell labelled with lysosome marker CD68 (red) from mock-infected organotypic slice.

Additional file 2: Video showing 3D confocal immunofluorescence analyses, reported in Fig. 4D, of mouse hippocampal organotypic slices transfected with EGFP. Video shows a representative microglial cell labelled with lysosome marker CD68 (red) of HSV-1-infected organotypic slice that is engulfed with EGFP neuronal material (green), revealing a colocalization signal (yellow).

Additional file 3: Video showing 3D confocal immunofluorescence analyses, reported in Fig. 4D, of mouse hippocampal organotypic slices transfected with EGFP. Video shows a representative microglial cell labelled with lysosome marker CD68 (red) of mock-infected organotypic slice treated with C3 Ab.

Additional file 4: Video showing 3D confocal immunofluorescence analyses, reported in Fig. 4D, of mouse hippocampal organotypic slices transfected with EGFP. Video shows a representative microglial cell labelled with lysosome marker CD68 (red) of HSV-1-infected organotypic slice treated with C3Ab that is engulfed with EGFP neuronal material (green), revealing a colocalization signal (yellow) that is decreased with respect to HSV-1.

Acknowledgements
The authors acknowledge Dr. Emanuela D'Amore, Dr. Mauro Valeri, and Andrea Martinelli (Istituto Superiore di Sanità, Centre for Animal Research and Welfare) for their valuable animal care support and Prof. Maria D'Erme (Department of Biochemical Sciences, Sapienza University) for kindly providing the BV2 microglial cell line. GDC and CG received funds from the European Union Next-GenerationEU- National Recovery and Resilience Plan (NRRP)- MISSION 4 COMPONENT 2, INVESTMENT 1.1, through the Ministry of University and Research (MUR), CALL PRIN 2022 D.D. 104 02-02-2022, PROJECT 2022ZYLB7B, CUP B53D23003770006 (for GDC), and CUP J53D23001290008 (for CG). The funder had no role in study design, data collection and analysis, decision to publish, or preparation of the manuscript.

Authors' contributions
Conceptualization: MTM and GDC. Investigation: MTM, VP, FZ, FP, CS, CR, MEM, RP. Formal analysis: MTM, VP, RP, CR, GDC. Visualization: MTM, VP, FZ and CR. Writing - Original Draft: MTM and GDC. Writing - Review & Editing: VP, ATP, CG and GDC. Supervision: ATP and GDC. Funding acquisition: CG and GDC. All authors read and approved the final manuscript.

Funding
GDC and CG received funds from the European Union Next-GenerationEU-National Recovery and Resilience Plan (NRRP)- MISSION 4 COMPONENT 2, INVESTMENT 1.1, through the Ministry of University and Research (MUR), CALL PRIN 2022 D.D. 104 02-02-2022, PROJECT 2022ZYLB7B (CUP B53D2300377 0006 for GDC, and CUP J53D23001290008 for CG). The funder had no role in study design, data collection and analysis, decision to publish, or manuscript preparation.

Data availability
No datasets were generated or analyzed during the current study.

Declarations

Ethics approval and consent to participate
All the experimental protocols used in the present study complied with the European Guide for the Care and Use of Laboratory Animals and institutional

guidelines and with the Italian legislation on animal experimentation (Decreto legislativo n. 26/2014, Direttiva UE 63/2010). Experimental protocols were reviewed by the Animal Welfare Body (Istituto Superiore Sanità and Università Cattolica) and authorized by the Italian Ministry of Health (code numbers D9997.N.GRQ and 934/2021-PR).

Consent for publication
Not applicable.

Competing interests
The authors declare no competing interests.

Author details
[1]Institute of Translational Pharmacology, Council of National Research, Rome, Italy
[2]Department of Public Health and Infectious Diseases, Sapienza University of Rome, Laboratory affiliated to Istituto Pasteur Italia-Fondazione Cenci Bolognetti, Rome, Italy
[3]Department of Infectious Diseases, Istituto Superiore di Sanità, Rome, Italy
[4]Department of Neuroscience, Università Cattolica del Sacro Cuore, Rome, Italy
[5]Fondazione Policlinico Universitario A. Gemelli IRCCS, Rome, Italy

Received: 12 September 2025 / Accepted: 11 February 2026
Published online: 20 February 2026

References

1. Kareem S, Jacob A, Mathew J, Quigg RJ, Alexander JJ. Complement: Functions, location and implications. Immunology. 2023;170:180–92. https://doi.org/10.1111/imm.13663.
2. Wang SSY, Tang H, Loe MWC, Yeo SC, Javaid MM. Complements and their role in systemic disorders. Cureus. 2024;16(1):52991. https://doi.org/10.7759/cureus.52991.
3. Schafer DP, Lehrman EK, Kautzman AG, Koyama R, Mardinly AR, Yamasaki R, et al. Microglia sculpt postnatal neural circuits in an activity and Complement-Dependent manner. Neuron. 2012;74:691–705. https://doi.org/10.1016/j.neuron.2012.03.026.
4. Stephan AH, Barres BA, Stevens B. The complement system: an unexpected role in synaptic pruning during development and disease. Annu Rev Neurosci. 2012;35:369–89. https://doi.org/10.1146/annurev-neuro-061010-113810.
5. Sekar A, Bialas AR, De Rivera H, Davis A, Hammond TR, Kamitaki N, et al. Schizophrenia risk from complex variation of complement component 4. Nature. 2016;530:177–83. https://doi.org/10.1038/nature16549.
6. Stevens B, Allen NJ, Vazquez LE, Howell GR, Christopherson KS, Nouri N, et al. The classical complement cascade mediates CNS synapse elimination. Cell. 2007;131:1164–78. https://doi.org/10.1016/j.cell.2007.10.036.
7. Mordelt A, De Witte LD. Microglia-mediated synaptic pruning as a key deficit in neurodevelopmental disorders: hype or hope? Curr Opin Neurobiol. 2023;79:102674. https://doi.org/10.1016/j.conb.2022.102674.
8. Wyatt SK, Witt T, Barbaro NM, Cohen-Gadol AA, Brewster AL. Enhanced classical complement pathway activation and altered phagocytosis signaling molecules in human epilepsy. Exp Neurol. 2017;295:184–93. https://doi.org/10.1016/j.expneurol.2017.06.009.
9. Figueiredo CP, Barros-Aragão FGQ, Neris RLS, Frost PS, Soares C, Souza INO, et al. Zika virus replicates in adult human brain tissue and impairs synapses and memory in mice. Nat Commun. 2019;10:3890. https://doi.org/10.1038/s41467-019-11866-7.
10. Gomez-Arboledas A, Acharya MM, Tenner AJ. The role of complement in synaptic pruning and neurodegeneration. ImmunoTargets Ther. 2021;10:373–86. https://doi.org/10.2147/ITT.S305420.
11. Vasek MJ, Garber C, Dorsey D, Durrant DM, Bollman B, Soung A, et al. A complement–microglial axis drives synapse loss during virus-induced memory impairment. Nature. 2016;534:538–43. https://doi.org/10.1038/nature18283.
12. Düsedau HP, Steffen J, Figueiredo CA, Boehme JD, Schultz K, Erck C, et al. Influenza A virus (H1N1) infection induces microglial activation and Temporal dysbalance in glutamatergic synaptic transmission. mBio. 2021;12:e01776–21. https://doi.org/10.1128/mBio.01776-21.
13. Fontes-Dantas FL, Fernandes GG, Gutman EG, De Lima EV, Antonio LS, Hammerle MB, et al. SARS-CoV-2 Spike protein induces TLR4-mediated long-term cognitive dysfunction recapitulating post-COVID-19 syndrome in mice. Cell Rep. 2023;42:112189. https://doi.org/10.1016/j.celrep.2023.112189.
14. Hong S, Beja-Glasser VF, Nfonoyim BM, Frouin A, Li S, Ramakrishnan S, et al. Complement and microglia mediate early synapse loss in alzheimer mouse models. Science. 2016;352:712–6. https://doi.org/10.1126/science.aad8373.
15. Zhang J, Zhang Y, Wang J, Xia Y, Zhang J, Chen L. Recent advances in alzheimer's disease: mechanisms, clinical trials and new drug development strategies. Signal Transduct Target Ther. 2024;9:211. https://doi.org/10.1038/s41392-024-01911-3.
16. Scheltens P, De Strooper B, Kivipelto M, Holstege H, Chételat G, Teunissen CE, et al. Alzheimer's disease. Lancet. 2021;397:1577–90. https://doi.org/10.1016/S0140-6736(20)32205-4.
17. Sandoval C, Lee J, Toth B, Nagaraj R, Schauer SP, Hoffman J, et al. CSF complement proteins are elevated in prodromal to moderate alzheimer's disease patients and are not altered by the anti-tau antibody semorinemab. Alzheimers Dement. 2024;20:7940–53. https://doi.org/10.1002/alz.14271.
18. Zhou J, Wang Z-B, Sun Y, Fu Y, Li D, Tan L. Cerebrospinal fluid complement 4 levels were associated with alzheimer's disease pathology and cognition in Non-Demented elderly. J Alzheimer's Dis. 2023;96:1071–81. https://doi.org/10.3233/JAD-230513.
19. Dejanovic B, Huntley MA, De Mazière A, Meilandt WJ, Wu T, Srinivasan K, et al. Changes in the synaptic proteome in tauopathy and rescue of Tau-Induced synapse loss by C1q antibodies. Neuron. 2018;100:1322–36. https://doi.org/10.1016/j.neuron.2018.10.014.
20. Marcocci ME, Napoletani G, Protto V, Kolesova O, Piacentini R, Li Puma DD, et al. Herpes simplex Virus-1 in the brain: the dark side of a sneaky infection. Trends Microbiol. 2020;28:808–20. https://doi.org/10.1016/j.tim.2020.03.003.
21. De Chiara G, Marcocci ME, Civitelli L, Argnani R, Piacentini R, Ripoli C, et al. APP processing induced by herpes simplex virus type 1 (HSV-1) yields several APP fragments in human and rat neuronal cells. PLoS ONE. 2010;5:e13989. https://doi.org/10.1371/journal.pone.0013989.
22. Li Puma DD, Piacentini R, Leone L, Gironi K, Marcocci ME, De Chiara G, et al. Herpes simplex virus Type-1 infection impairs adult hippocampal neurogenesis via Amyloid-β protein accumulation. Stem Cells. 2019;37:1467–80. https://doi.org/10.1002/stem.3072.
23. Napoletani G, Protto V, Marcocci ME, Nencioni L, Palamara AT, De Chiara G. Recurrent herpes simplex virus type 1 (HSV-1) infection modulates neuronal aging marks in in vitro and in vivo models. Int J Mol Sci. 2021;22:6279. https://doi.org/10.3390/ijms22126279.
24. Piacentini R, Li Puma DD, Ripoli C, Elena Marcocci M, De Chiara G, Garaci E, et al. Herpes simplex virus type-1 infection induces synaptic dysfunction in cultured cortical neurons via GSK-3 activation and intraneuronal amyloid-β protein accumulation. Sci Rep. 2015;5:15444. https://doi.org/10.1038/srep15444.
25. De Chiara G, Piacentini R, Fabiani M, Mastrodonato A, Marcocci ME, Limongi D, et al. Recurrent herpes simplex virus-1 infection induces hallmarks of neurodegeneration and cognitive deficits in mice. PLoS Pathog. 2019;15:e1007617. https://doi.org/10.1371/journal.ppat.1007617.
26. Protto V, Miteva MT, Iannuzzi F, Marcocci ME, Li Puma DD, Piacentini R, et al. HSV-1 infection induces phosphorylated Tau propagation among neurons via extracellular vesicles. mBio. 2024;15:e01522–24. https://doi.org/10.1128/mbio.01522-24.
27. Li Puma DD, Colussi C, Bandiera B, Puliatti G, Rinaudo M, Cocco S, et al. Interleukin 1β triggers synaptic and memory deficits in herpes simplex virus type-1-infected mice by downregulating the expression of synaptic plasticity-related genes via the epigenetic MeCP2/HDAC4 complex. Cell Mol Life Sci. 2023;80:172. https://doi.org/10.1007/s00018-023-04817-5.
28. Renna P, Ripoli C, Dagliyan O, Pastore F, Rinaudo M, Re A, et al. Engineering a switchable single-chain TEV protease to control protein maturation in living neurons. Bioeng Transl Med. 2022;7:e10292. https://doi.org/10.1002/btm2.10292.
29. Ripoli C, Dagliyan O, Renna P, Pastore F, Paciello F, Sollazzo R, et al. Engineering memory with an extrinsically disordered kinase. Sci Adv. 2023;9:eadh1110. https://doi.org/10.1126/sciadv.adh1110.
30. Killington RA, Powell KL. Growth, assay and purification of herpes viruses. In: Mahy BWJ, editor. Virology: a practical approach. IRL Press at Oxford University; 1991. pp. 207–36.
31. D'Arcangelo G, Grossi D, De Chiara G, De Stefano MC, Cortese G, Citro G, et al. Glutamatergic neurotransmission in a mouse model of Niemann–Pick type C

disease. Brain Res. 2011;1396:11–9. https://doi.org/10.1016/j.brainres.2011.04.020.
32. Fan R, Tenner AJ. Complement C1q expression induced by Aβ in rat hippocampal organotypic slice cultures. Exp Neurol. 2004;185:241–53. https://doi.org/10.1016/j.expneurol.2003.09.023.
33. Hernandez-Encinas E, Aguilar-Morante D, Morales-Garcia JA, Gine E, Sanz-SanCristobal M, Santos A, et al. Complement component 3 (C3) expression in the hippocampus after excitotoxic injury: role of C/EBPβ. J Neuroinflammation. 2016;13:276. https://doi.org/10.1186/s12974-016-0742-0.
34. Habif M, Do Carmo S, Báez MV, Colettis NC, Cercato MC, Salas DA, et al. Early Long-Term memory impairment and changes in the expression of synaptic Plasticity-Associated Genes, in the McGill-R-Thy1-APP rat model of Alzheimer's-Like brain amyloidosis. Front Aging Neurosci. 2021;12:585873. https://doi.org/10.3389/fnagi.2020.585873.
35. Zhou S, Du X, Xie J, Wang J. Interleukin-6 regulates iron-related proteins through c-Jun N-terminal kinase activation in BV2 microglial cell lines. PLoS ONE. 2017;12:e0180464. https://doi.org/10.1371/journal.pone.0180464.
36. Gao T, Huang F, Wang W, Xie Y, Wang B. Interleukin-10 genetically modified clinical-grade mesenchymal stromal cells markedly reinforced functional recovery after spinal cord injury via directing alternative activation of macrophages. Cell Mol Biol Lett. 2022;27:27. https://doi.org/10.1186/s11658-022-00325-9.
37. Piano I, Votta A, Colucci P, Corsi F, Vitolo S, Cerri C, et al. Anti-inflammatory reprogramming of microglia cells by metabolic modulators to counteract neurodegeneration; a new role for Ranolazine. Sci Rep. 2023;13:20138. https://doi.org/10.1038/s41598-023-47540-8.
38. Santos ARA, Duarte CB. Validation of internal control genes for expression studies: effects of the neurotrophin BDNF on hippocampal neurons. J Neurosci Res. 2008;86:3684–92. https://doi.org/10.1002/jnr.21796.
39. Komoroski BJ, Zhang S, Cai H, Hutzler JM, Frye R, Tracy TS, INDUCTION AND INHIBITION OF CYTOCHROMES P450 BY THE ST. JOHN'S WORT CONSTITUENT HYPERFORIN IN HUMAN HEPATOCYTE CULTURES, et al. Drug Metab Dispos. 2004;32:512–8. https://doi.org/10.1124/dmd.32.5.512.
40. Livak KJ, Schmittgen TD. Analysis of relative gene expression data using Real-Time quantitative PCR and the 2 – ΔΔCT method. Methods. 2001;25:402–8. https://doi.org/10.1006/meth.2001.1262.
41. Ripoli C, Piacentini R, Riccardi E, Leone L, Li Puma DD, Bitan G, et al. Effects of different amyloid β-protein analogues on synaptic function. Neurobiol Aging. 2013;34:1032–44. https://doi.org/10.1016/j.neurobiolaging.2012.06.027.
42. Schartz ND, Tenner AJ. The good, the bad, and the opportunities of the complement system in neurodegenerative disease. J Neuroinflammation. 2020;17:354. https://doi.org/10.1186/s12974-020-02024-8.
43. Shinjyo N, Kagaya W, Pekna M. Interaction between the complement system and infectious Agents – A potential mechanistic link to neurodegeneration and dementia. Front Cell Neurosci. 2021;15:710390. https://doi.org/10.3389/fncel.2021.710390.
44. Whittaker V, Michaelson I, Kirkland R. The separation of synaptic vesicles from nerve-ending particles ('synaptosomes'). Biochem J. 1964;90:293–303. https://doi.org/10.1042/bj0900293.
45. Kumar S. Synaptosome micrornas: emerging synapse players in aging and alzheimer's disease. Neural Regen Res. 2023;18:1275. https://doi.org/10.4103/1673-5374.360172.
46. Zhao H, Lv Y, Xu J, Song X, Wang Q, Zhai X, et al. The activation of microglia by the complement system in neurodegenerative diseases. Ageing Res Rev. 2025;104:102636. https://doi.org/10.1016/j.arr.2024.102636.
47. Zotova E, Bharambe V, Cheaveau M, Morgan W, Holmes C, Harris S, et al. Inflammatory components in human alzheimer's disease and after active amyloid-β42 immunization. Brain. 2013;136:2677–96. https://doi.org/10.1093/brain/awt210.
48. Kostavasili I, Sahu A, Friedman HM, Eisenberg RJ, Cohen GH, Lambris JD. Mechanism of complement inactivation by glycoprotein C of herpes simplex virus. J Immunol. 1997;158:1763–71.
49. Friedman HM, Cohen GH, Eisenberg RJ, Seidel CA, Cines DB. Glycoprotein C of herpes simplex virus 1 acts as a receptor for the C3b complement component on infected cells. Nature. 1984;309:633–5. https://doi.org/10.1038/309633a0.
50. Da Costa XJ, Brockman MA, Alicot E, Ma M, Fischer MB, Zhou X, et al. Humoral response to herpes simplex virus is complement-dependent. Proc Natl Acad Sci. 1999;96:12708–12. https://doi.org/10.1073/pnas.96.22.12708.
51. Bibert S, Piret J, Quinodoz M, Collinet E, Zoete V, Michielin O, et al. Herpes simplex encephalitis in adult patients with MASP-2 deficiency. PLoS Pathog. 2019;15:e1008168. https://doi.org/10.1371/journal.ppat.1008168.
52. Eriksson CE, Studahl M, Bergström T. Acute and prolonged complement activation in the central nervous system during herpes simplex encephalitis. J Neuroimmunol. 2016;295–296:130–8. https://doi.org/10.1016/j.jneuroim.2016.04.013.
53. Shen Y, Li R, McGeer EG, McGeer PL. Neuronal expression of mRNAs for complement proteins of the classical pathway in alzheimer brain. Brain Res. 1997;769:391–5. https://doi.org/10.1016/S0006-8993(97)00850-0.
54. Thomas A, Gasque P, Vaudry D, Gonzalez B, Fontaine M. Expression of a complete and functional complement system by human neuronal cells in vitro. Int Immunol. 2000;12:1015–23. https://doi.org/10.1093/intimm/12.7.1015.
55. Veerhuis R, Janssen I, De Groot CJA, Van Muiswinkel FL, Hack CE, Eikelenboom P. Cytokines associated with amyloid plaques in alzheimer's disease brain stimulate human glial and neuronal cell cultures to secrete early complement Proteins, but not C1-Inhibitor. Exp Neurol. 1999;160:289–99. https://doi.org/10.1006/exnr.1999.7199.
56. Veerhuis R, Nielsen HM, Tenner AJ. Complement in the brain. Mol Immunol. 2011;48:1592–603. https://doi.org/10.1016/j.molimm.2011.04.003.
57. Yu JX, Bradt BM, Cooper NR. Constitutive expression of Proinflammatory complement components by subsets of neurons in the central nervous system. J Neuroimmunol. 2002;123:91–101. https://doi.org/10.1016/S0165-5728(01)00483-0.
58. Yirün A, Çakır DA, Sanajou S, Erdemli Köse SB, Özyurt AB, Zeybek D, et al. Evaluation of the effects of herpes simplex glycoprotein B on complement system and cytokines in in vitro models of alzheimer's disease. J Appl Toxicol. 2023;43:1368–78. https://doi.org/10.1002/jat.4471.
59. Trebesova H, Grilli M, Synaptosomes. A functional tool for studying neuroinflammation. Encyclopedia. 2023;3:406–18. https://doi.org/10.3390/encyclopedia3020027.
60. Deivasigamani S, Miteva MT, Natale S, Gutierrez-Barragan D, Basilico B, Di Angelantonio S, et al. Microglia complement signaling promotes neuronal elimination and normal brain functional connectivity. Cereb Cortex. 2023;33:10750–60. https://doi.org/10.1093/cercor/bhad313.
61. Wu J, Bie B, Foss JF, Naguib M. Amyloid Fibril-Induced astrocytic glutamate transporter disruption contributes to complement C1q-Mediated microglial pruning of glutamatergic synapses. Mol Neurobiol. 2020;57:2290–300. https://doi.org/10.1007/s12035-020-01885-7.
62. Piacentini R, Civitelli L, Ripoli C, Marcocci ME, De Chiara G, Garaci E, et al. HSV-1 promotes Ca2+-mediated APP phosphorylation and Aβ accumulation in rat cortical neurons. Neurobiol Aging. 2011;32:2323.e13-2323.e26. https://doi.org/10.1016/j.neurobiolaging.2010.06.009.
63. Liddelow SA, Guttenplan KA, Clarke LE, Bennett FC, Bohlen CJ, Schirmer L, et al. Neurotoxic reactive astrocytes are induced by activated microglia. Nature. 2017;541:481–7. https://doi.org/10.1038/nature21029.
64. Chung W-S, Clarke LE, Wang GX, Stafford BK, Sher A, Chakraborty C, et al. Astrocytes mediate synapse elimination through MEGF10 and MERTK pathways. Nature. 2013;504:394–400. https://doi.org/10.1038/nature12776.
65. Wang Z, Liu J, Han J, Zhang T, Li S, Hou Y, et al. Herpes simplex virus 1 accelerates the progression of alzheimer's disease by modulating microglial phagocytosis and activating NLRP3 pathway. J Neuroinflammation. 2024;21:176. https://doi.org/10.1186/s12974-024-03166-9.
66. West EE, Kemper C. Complosome — the intracellular complement system. Nat Rev Nephrol. 2023;19:426–39. https://doi.org/10.1038/s41581-023-00704-1.
67. Martin C, Aguila B, Araya P, Vio K, Valdivia S, Zambrano A, et al. Inflammatory and neurodegeneration markers during asymptomatic HSV-1 reactivation. J Alzheimers Dis. 2014;39:849–59. https://doi.org/10.3233/JAD-131706.
68. Wozniak MA, Itzhaki RF, Shipley SJ, Dobson CB. Herpes simplex virus infection causes cellular β-amyloid accumulation and secretase upregulation. Neurosci Lett. 2007;429:95–100. https://doi.org/10.1016/j.neulet.2007.09.077.
69. Zelek WM, Bevan RJ, Nimmo J, Dewilde M, De Strooper B, Morgan BP. Brain-penetrant complement Inhibition mitigates neurodegeneration in an alzheimer's disease mouse model. Brain. 2025;148:941–54. https://doi.org/10.1093/brain/awae278.

Publisher's note